Marine Pollution Bulletin 132 (2018) 5–25

Contents lists available at ScienceDirect

Marine Pollution Bulletin

journal homepage: www.elsevier.com/locate/marpolbul

Numerical simulations of debris drift from the Great Japan Tsunami of 2011 and their verification with observational reports☆

Nikolai Maximenko[a,*], Jan Hafner[a], Masafumi Kamachi[b], Amy MacFadyen[c]

[a] International Pacific Research Center, School of Ocean & Earth Science & Technology, University of Hawaii at Manoa, United States
[b] Japan Agency for Marine-Earth Science and Technology, Japan
[c] US National Oceanic and Atmospheric Administration, Office of Response and Restoration, Emergency Response Division, United States

ARTICLE INFO

Keywords:
Numerical modeling
Data analysis
Ocean surface circulation
Marine debris drift
Tsunami debris
Debris pathways
Sensitivity to windage
Debris reports
Model calibration/validation
Model-data comparison
New methods

ABSTRACT

A suite of five ocean models is used to simulate the movement of floating debris generated by the Great Japan Tsunami of 2011. This debris was subject to differential wind and wave-induced motion relative to the ambient current (often termed "windage") which is a function of the shape, size, and buoyancy of the individual debris items. Model solutions suggest that during the eastward drift across the North Pacific the debris became "stratified" by the wind so that objects with different windages took different paths: high windage items reached North America in large numbers the first year, medium windage items recirculated southwest toward Hawaii and Asia, and low windage items collected in the Subtropical Gyre, primarily in the so-called "garbage patch" area located northeast of Hawaii and known for high concentrations of microplastics. Numerous boats lost during the tsunami were later observed at sea and/or found on the west coast of North America: these observations are used to determine optimal windage values for scaling the model solutions. The initial number of boats set adrift during the tsunami is estimated at about 1000, while about 100 boats are projected to still float in year 2018 with an e-folding decay of 2 to 8 years.

1. Introduction

The tragic March 11, 2011, Great Japan Tsunami took more than 15,000 lives and generated an estimated 1.5 million tons of floating debris off eastern Honshu (Ministry of the Environment, Japanese Agency, 2012), an amount comparable to the annual budget of plastic marine debris generated in and along shores of the entire North Pacific (Jambeck et al., 2015). Pathways of general marine debris are hard to study, in part because the debris sources are scattered over large distances and long periods of time. Accumulation regions for microplastics (particles of fragmented plastic less than 1 cm in size) have been studied more than those of other types of debris (Law et al., 2010; Eriksen et al., 2013; van Sebille et al., 2015), but account for only a tiny fraction of the debris input. The Great Japan Tsunami provided a unique opportunity to better understand how ocean debris drifts by following individual items and "waves" of debris deposition around the North Pacific. Even in areas heavily polluted with general debris from routine activities, many Japan tsunami marine debris (JTMD) items could be easily identified. In some places, "waves" of JTMD were obvious because of a dramatic increase in all categories of debris (Murray et al., 2018).

The unique dataset collected over the past six years has revealed the complex dynamics of JTMD travel across the ocean (Carlton et al., 2017). At the same time, it has also revealed weaknesses of the present observing system that largely relies on motivated observers, whose availability varies widely and is sparse in many parts of the Pacific and its shores. Numerical models were used to fill in the gaps in observations and help to construct the "big picture" of JTMD transport and deposition.

Presented here are results from five different ocean models and systems, their calibration/validation using observational reports, and their estimates of the total amounts and fate of JTMD.

The paper is organized as follows. The next section describes the models and setups of the numerical experiments as well as the model initializations and the unification of model solutions for comparative analyses. Section 3 describes the dynamics of JTMD in the model solutions. Section 4 introduces the observational dataset and compares the distributions of JTMD boat reports at sea and on the US/Canada west coast with model concentrations and fluxes. In Section 5, optimally scaled model solutions show estimates of the initial number of

☆ This is one of the papers from the special issue of Marine Pollution Bulletin on "The effect of marine debris caused by the Great Tsunami of 2011." The special issue was supported by funding provided by the Ministry of the Environment of Japan (MOE) through the North Pacific Marine Science Organization (PICES).

* Corresponding author.
E-mail address: maximenk@hawaii.edu (N. Maximenko).

https://doi.org/10.1016/j.marpolbul.2018.03.056
Received 22 June 2017; Received in revised form 28 February 2018; Accepted 28 March 2018
Available online 02 May 2018

JTMD boats and their possible fate. Section 6 concludes the paper and discusses some remaining questions and future work.

2. Model configurations

A suite of five numerical models, developed independently by participating groups in Japan and the United States, was run to produce an ensemble of solutions that were used to characterize the drift of JTMD, compare with observational reports and assess robustness of conclusions. In each model, the velocity of the debris drift was calculated from surface currents; the effect of the direct wind-forcing on the drift was accounted for by adding to the drift a fraction of the wind velocity, characterized by a "windage" parameter. Because the models represent near-surface, wind-driven currents differently, the same object could have different windage values in different models.

2.1. SCUD model

The *SCUD* model (Surface CUrrents from Diagnostic) was developed at the International Pacific Research Center (IPRC) of University of Hawaii, USA, (Maximenko and Hafner, 2010) to produce high-resolution maps of ocean surface currents, consistent with trajectories of the sparse array of satellite-tracked drifting buoys, drogued at 15-meter depth. The model uses two satellite data sets: sea level anomaly from altimetry, processed by the AVISO, and surface winds from QuikSCAT (1999–2009) and ASCAT (since 2007) satellites (the latter was calibrated using nearly two years of the overlap with QuikSCAT). Model currents are calculated from a combination of the mean geostrophic flow, derived from the mean dynamic topography (Maximenko et al., 2009), its anomaly, and locally induced wind-driven currents. The latter implicitly include the Ekman currents, Stokes drift, and other motions correlated with the local wind. The model coefficients are tuned using velocities of nearly 20,000 drifting buoys of the Global Drifter Program[1] collocated in time and space with satellite observations. The SCUD model produces daily, near-real time and nearly global maps on a ¼-degree grid that are available on the IPRC/APDRC[2] servers. SCUD and its precursors were used to successfully describe the global distribution of microplastics (Maximenko et al., 2012). Model solutions helped to explain historical data (Law et al., 2010; van Sebille et al., 2015) and to coordinate expeditions that empirically verified the existence of garbage patches in the Southern Hemisphere (Eriksen et al., 2013).

2.2. SCUD-HYCOM model

The spatial grid of SCUD (1/4°) adequately resolves such important ocean scales as the deformation radius and size of mesoscale eddies in the North Pacific (Chelton et al., 2011); the resolution also corresponds to the parameters of the ocean observing system. However, such resolution may be too coarse for simulations in coastal areas and especially those around islands. To increase the resolution of JTMD drift in coastal areas and its accumulation on shorelines, the SCUD model was blended with HYCOM[3] (Bleck and Boudra, 1981) data, increasing the original ¼° grid of SCUD to 1/12°. The blending was limited to 100-km coastal bins with the relative weight of HYCOM progressively increasing toward the coast. An additional 100-km buffer zone that removed biases and adjusted the model's response to local winds was added to calibrate the current velocities of the two models. This buffer zone provided a seamless transition between the SCUD and HYCOM solutions. Hereafter, we will refer to this blended model as *SCUD-HYCOM*.

2.3. MOVE/K-7/SEA-GEARN system

The MOVE/K-7/SEA-GEARN (hereafter, *MOVE*) drift/dispersion model was created in Japan by a team of scientists from the Japan Agency for Marine-Earth Science and Technology (JAMSTEC), the Japan Atomic Energy Agency (JAEA), the Meteorological Research Institute (MRI) of the Japan Meteorological Agency (JMA), and the Japan Aerospace Exploration Agency (*JAXA*) in order to examine JTMD positions in the North Pacific as well as its landing sites and dates on coastlines. Numerical experiments included hindcasts from March 2011 to July 2013, followed by forecast runs through May 2016. The hindcasts were based on 3dVAR data assimilation in the North Pacific ocean general circulation model MOVE (Usui et al., 2006), operated by JMA/MRI. 3dVAR provides a kind of optimal interpolation in space, ignoring temporal variations and (for each time moment) processing observations fitting into the associated assimilation time window. The resolution of this model is 1/10° west of the dateline and relaxed to a 1/2° grid elsewhere. The model is forced by fluxes produced by the JMA's operational atmospheric system JCDAS. The forecast phase of simulations, including ocean currents and winds, was performed using the K7 atmosphere-ocean-land coupled system, operated by JAMSTEC, with a global 1° resolution (Sugiura et al., 2008). Kawamura et al. (2014) analyzed trajectories of 153,600 particles released offshore of Iwate, Miyagi, and Fukushima prefectures using the SEA-GEARN dispersion model, operated by JAEA. Results of the model have been also reported by the Japan Ministry of Environment (2014)[4].

2.4. FORA-WNP30 re-analysis

FORA-WNP30 (hereafter, *FORA*) is a 30-year, four-dimensional, variational ocean re-analysis of the western North Pacific. This dataset is produced with the MOVE/MRI·COM-4dVAR system. The ocean circulation model is MRI·COM (e.g., Tsujino et al., 2010) and the assimilation system is the same as that in MOVE except that the assimilation method is 4dVAR (Usui et al., 2015). Overall, FORA-WNP30 reproduces well the basic features of the interannual to decadal variability in the western North Pacific. 4dVAR is an optimum space-time interpolation and extrapolation of observational data, using a numerical model. Compared to 3dVAR, 4dVAR generally produces more accurate spatial patterns and temporal tendencies. Usui et al. (2017) provided a detailed description of the 4dVAR method adopted in the re-analysis, its validation through comparison with independent observations, and analyses of the interannual to decadal variability.

2.5. GNOME model

GNOME (General NOAA Operational Modeling Environment) is the modeling tool developed and used by the Office of Response and Restoration's (OR&R) Emergency Response Division (ERD) of the US National Oceanic and Atmospheric Administration (NOAA) to predict trajectories of oil, debris, and other floating marine pollutants.[5] GNOME is essentially a stand-alone particle tracking model and is not implicitly tied to a specific ocean model. In this application, GNOME utilized surface currents from the 1/12° operational HYCOM[6] model from the Naval Research Laboratory and 1/4° global wind product from the NOAA Blended Sea Winds.[7] After the Great Japan Tsunami of 2011, results of the GNOME hindcast experiments, based on trajectories of 40,000 particles, initialized at 8 sites along the Japan coast, were mapped with the NOAA Environmental Response Management Application (ERMA) and used to coordinate the response to potential JTMD.

[1] http://www.aoml.noaa.gov/phod/dac/index.php.
[2] http://apdrc.soest.hawaii.edu/.
[3] http://hycom.org/hycom/overview.
[4] http://www.kantei.go.jp/jp/singi/kaiyou/hyouryuu_eng/gaiyou.pdf.
[5] https://gnome.orr.noaa.gov/.
[6] http://www7320.nrlssc.navy.mil/GLBhycom1-12/skill.html.
[7] http://www.ncdc.noaa.gov/oa/rsad/air-sea/seawinds.html.

For this study, we calculated trajectories of more than 400,000 particles with start points distributed continuously along the east coast of Honshu Island. Calculations were repeated for 15 values of the windage parameter ranging between 0% and 5% of the wind speed. Turbulent diffusive processes that spread particles horizontally are simulated in GNOME by a random walk. A diffusion coefficient of 1 $m^2 s^{-1}$ was used to calculate random step lengths in the zonal and meridional directions from a uniform distribution. The current version of GNOME has no spatial variability in the horizontal diffusion, resulting in a uniform spreading of the particles over time.

2.6. Model initialization

Use of adequate initial model conditions is critical for successful simulations. The Japan Ministry of the Environment (JMoE) estimated that as much as 5 million tons of debris could have been created by the Great East Japan earthquake and tsunami of 2011, of which about 1.5 million tons could have become floating debris; information about debris composition and distribution of sources along the coastline, however, is largely unavailable. To overcome these unknowns, we ran the models under a range of parameters, covering all main types of JTMD, and analyzed reports on the height of tsunami waves and extent of destruction they caused.

Generation of JTMD was a complex, multi-phase process: it started with an inundation of coastal areas by tsunami waves, damage to the structures, and was followed by floating and suspended debris being washed back into the ocean with retreating turbulent waters. The impact of the tsunami (Kako et al., 2018) depended not only on wave height but also, among other things, on the ocean and land topography, and resilience of buildings and structures. The amounts and types of generated debris also depend on the degree of development and types of main activities (fishing, recreational, residential, industrial, etc.) in the region. In this study, we used recent data on the number of homes destroyed by the tsunami, from municipal services and the Asahi Shimbun newspaper (H. Maki, National Institute for Environmental Studies, Japan, personal communication). Together, these reports cover the entire eastern shore of Honshu (Fig. 1a). We found that the two sources complement each other with good agreement for the 19 towns that were included in both data sets (for which we used the average value). The merged dataset, shown in Fig. 1, includes 43 towns and villages, in which a total of 100,554 homes were reported damaged or destroyed by the tsunami. The greatest devastation was reported between 37.5°N and 39.8°N (the entire coast of Miyagi prefecture, the southern part of Iwate prefecture and the northern part of Fukushima prefecture) with a pronounced peak near 38.5°N.

To calculate the distribution of JTMD source with latitude, shown in Fig. 1b with a black line, a Gaussian filter with a 1/4° half-width was applied to the discrete data (blue bars in Fig. 1b). Compared to the model results obtained by Maximenko et al. (2015) in previous studies with homogeneous or discrete sources, the continuous "source function" used in this study added more realism to the numerical experiments and helped unify settings across the models.

2.7. Model unification

To facilitate meaningful, quantitative comparisons between the five very different models, we set the range of model parameters as close as possible and treated secondary processes in a similar manner. For example, the possibility for model debris to re-float after stranding on shorelines was switched off in all models; particles and tracers that crossed from ocean bins into coastal bins were kept in the coastal bins. To account for "windage" or "leeway" effects (motion of floating objects due to direct wind forcing), the models were forced with a corresponding fraction (between 0 and 5% in GNOME and between 0 and 6% in the four other models) of wind velocity, and with current vectors to produce full drift velocities. Tracer experiments based on ocean

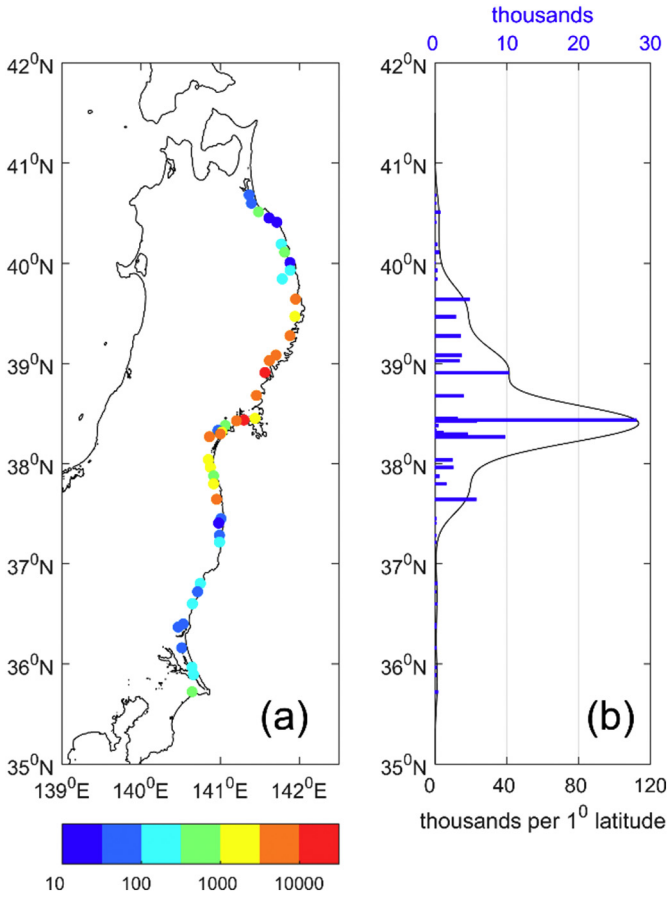

Fig. 1. (a) Number of reported damaged homes. (Note the nonlinear color scale.) (b) Distribution with latitude of reports (blue bars) and probability density function (black line), calculated with a Gaussian filter of a 1/4° half-width, and used to initiate model experiments. Units are thousands and thousands per degree of latitude. (For interpretation of the references to color in this figure legend, the reader is referred to the web version of this article.)

currents from SCUD, SCUD-HYCOM, MOVE and FORA models were executed at IPRC using the same numerical algorithm. In all models, the same total amount of tracer was released at 13 sites along the east coast of Honshu, separated by 1/2° latitude and weighted with the source function, shown in Fig. 1b.

Because GNOME uses particles for its simulations, inter-model comparison required converting the particle distributions obtained from the model into tracer densities equivalent to those obtained from the other models. To accomplish this, we initialized as many as 400,000 particles (10 times of the number used in initial response modeling effort) scattered uniformly among all near-shore HYCOM model bins east of Japan (between 35°N and 41°N). Each particle was assigned a weight according to the latitude of its start position, so that together the weighted source of the particles corresponded to the source profile in Fig. 1b.

For the conversion to tracer density, each particle was replaced by a co-located tracer cloud with a Gaussian "bell" shape decaying at radius σ and limited by a radius of three σ. To derive the optimal value for σ, we performed additional experiment, in which GNOME was forced by the same surface currents and winds as SCUD-HYCOM. The latter model was selected because its grid coincides with the HYCOM grid, used in the GNOME experiments. Calculations were made only for a windage parameter of 2.75% — a medium-windage tracer in the JTMD simulation. Optimal σ was determined by minimizing the relevant difference between tracer gradients in the two models. For different years σ varied between 30 and 50 km and we chose σ = 40 km as a constant optimal

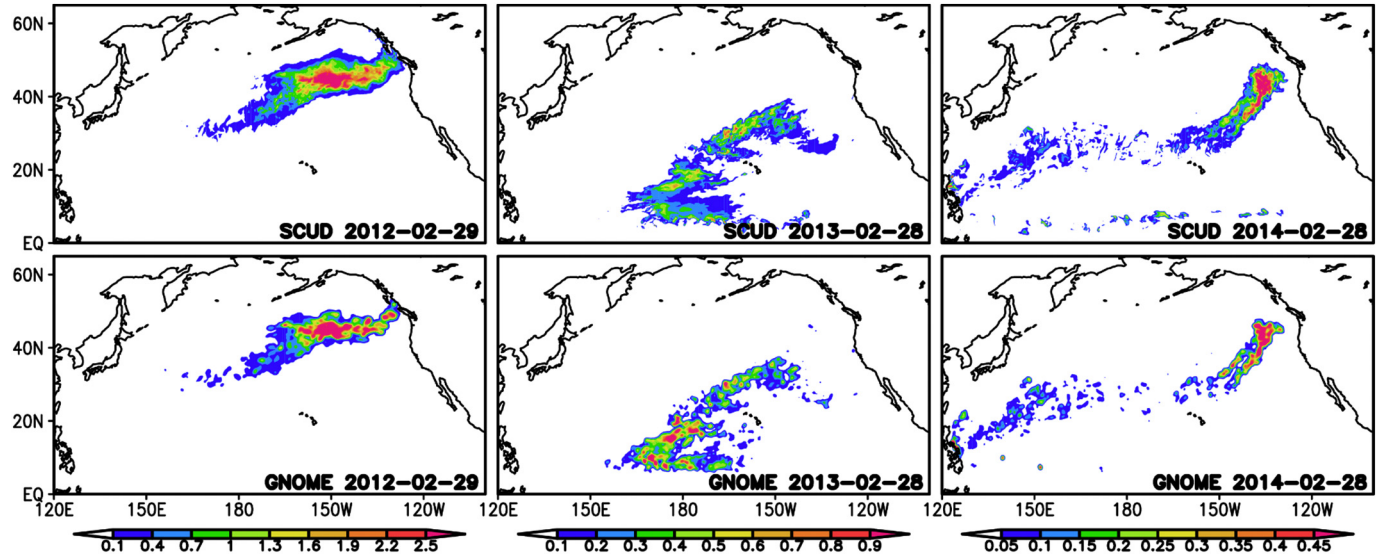

Fig. 2. Evolution of JTMD tracer concentration with 2.75% windage (upper row) converted from the GNOME particle experiments and (lower row) the SCUD-HYCOM tracer simulations, using same surface currents and winds Shown are maps, corresponding to February 29, 2012, February 28, 2013, and February 28, 2014. Units are conventional and color scale varies with time.

value. Fig. 2 shows that such conversion produces GNOME maps resembling tracer maps for SCUD-HYCOM as would be expected when using the same forcing. Subsequently, this same procedure was applied to all GNOME solutions.

3. Model solutions

The temporal evolution of the five model solutions formatted in similar ways is illustrated in Figs. 3–7. To facilitate comparisons, we included only tracer values ranging from 0 to 5% for all models. We use colors to visualize the complex composition of multi-windage tracers with red/green/blue corresponding to high/medium/low-windage values.

The model solutions are consistent with each other in many aspects. In 2011, all model "clouds" move eastward away from Japan and toward North America, consistent with the pattern of eastward surface currents (e.g., Niiler et al., 2003) separating the subtropical and subpolar gyres. The strongest jet, with velocities over 1 m/s, starts as an extension of the Kuroshio Current flowing along the southern coast of Japan. The signature of the Kuroshio Extension is clearly evident on the September 2, 2011 maps along the hind (western) edges of the tracer clouds in Figs. 3–6. A zonal band of "clear water" along 35°N that separates higher concentrations of mostly low-windage (blue) tracer north and south of it, marks the position of the Kuroshio Extension axis. Further east, the jet broadens and weakens, becoming the North Pacific Current.

As the tracer moves east, it becomes "stratified" by westerly winds, prevailing in the northern North Pacific. High-windage debris, accelerated by these winds, reaches North American shores around the end of 2011, consistent with the timing of first reports of JTMD there. Note that the February 29, 2012 maps suggest that the greatest deposition of high-windage JTMD was in Alaska. Given the low-population density and severe winter storms, most of the JTMD stranded on Alaska shorelines was not documented until the next summer or even the following years (Murray et al., 2018). Alaska is also a common destination of high-windage debris such as styrofoam fishing buoys, so that the first arrival of JTMD did not raise immediate concern and response. Importantly, the models suggest that most of the high-windage debris washed ashore on the West Coast before summer 2012 and therefore was mostly removed from the ocean. Only a small fraction recirculated south- and then westward toward Asia. Also, if the models were including re-floatation of debris by storms, some high-windage tracer could float on the Alaska Stream, toward the Aleutian Islands and Russia.

The September 1, 2012 maps in Figs. 3 to 7 suggest that upon reaching North America, much of the medium-windage tracer (green colors) recirculates southwestward toward the Hawaiian Islands. This is consistent with the timing of confirmed reports from Hawaii in Fall 2012. Remarkably, JTMD arrived in Hawaii not from the west but from the east.

Low-windage tracer, originally "tailing" the high-windage tracer, moves by the end of 2013 toward an area northeast of Hawaii known for elevated concentrations of microplastics, the so-called Garbage Patch (Moore et al., 2001). Kubota (1994) studied the dynamics of the associated convergence of surface currents and Maximenko et al. (2012) used trajectories of real drifting buoys to reproduce numerically the process of the garbage patch formation in the North Pacific and in four other subtropical oceans. They showed that drifters (which would correspond to a low-windage debris in our terminology) can reside in this region for a very long time and occasionally spill out of the patch and drift to the shorelines of Hawaii and North America.

Though the model solutions are overall similar, a careful look reveals significant differences. For example, the maps in Fig. 4 are less diffuse than those in Fig. 3. This is because SCUD-HYCOM uses a finer grid (10 km compared to 25 km) than SCUD and the numerical subgrid mixing is stronger for a coarser grid. Indeed, the meridional spread of the tracer by September 2, 2011, is narrower in SCUD-HYCOM (Fig. 4) than in SCUD (Fig.3). However, this difference disappears in the following year, probably because of strong mixing by mesoscale eddies resolved in both models. Also it is important to note that adding the near-shore dynamics to the initial evolution of the tracer by blending SCUD with HYCOM does not significantly change the structure of SCUD's solution in the open ocean, probably because the predominantly eastward currents and westerly winds promptly move JTMD offshore.

Similar differences can be found between the MOVE (Fig. 5) and FORA (Fig. 6) model solutions. The MOVE tracer covers in 2011 and early 2012 a greater area than FORA, indicating more eddy energy or other variability in currents and winds. Compared to the other models, the tracer in the MOVE solution maps on September 2, 2011, and February 29, 2012, extends farther north and seem to even reach the Aleutian Islands. The lack of reports from the Aleutian Islands may be due to a lack of observers and can't be used to verify MOVE. The quality

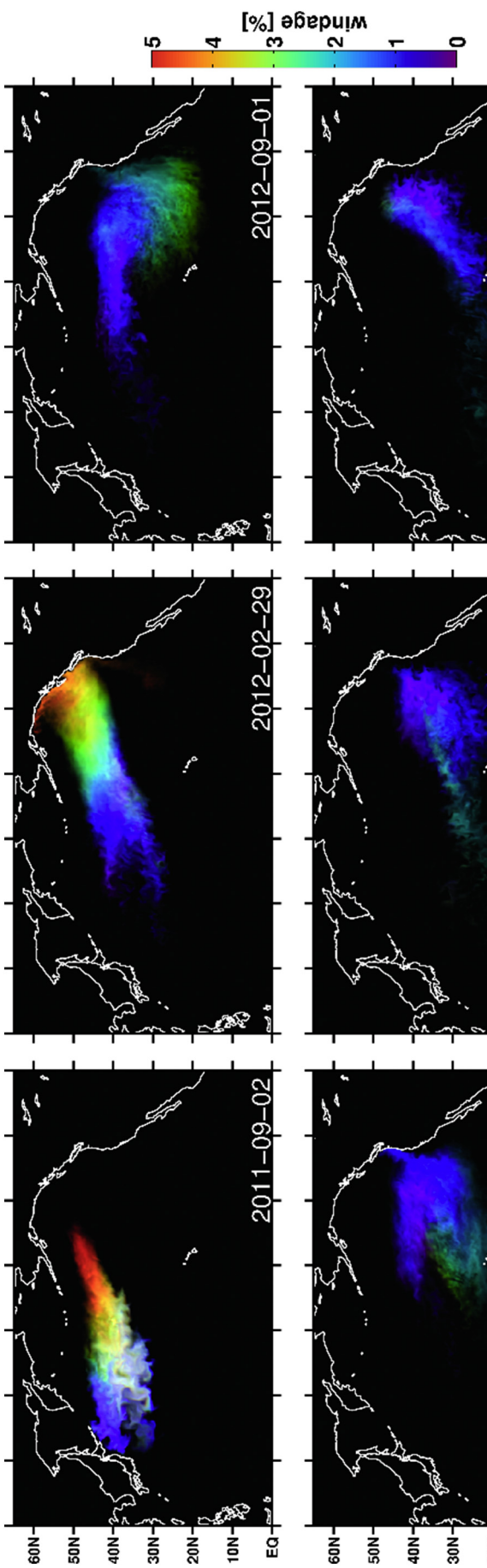

Fig. 3. Evolution of JTMD tracer concentration in the SCUD model simulations. Colors indicate windage of the debris. Shown are maps, corresponding to September 2, 2011, February 29, 2012, September 1, 2012, February 28, 2013, September 1, 2013, and February 28, 2014.

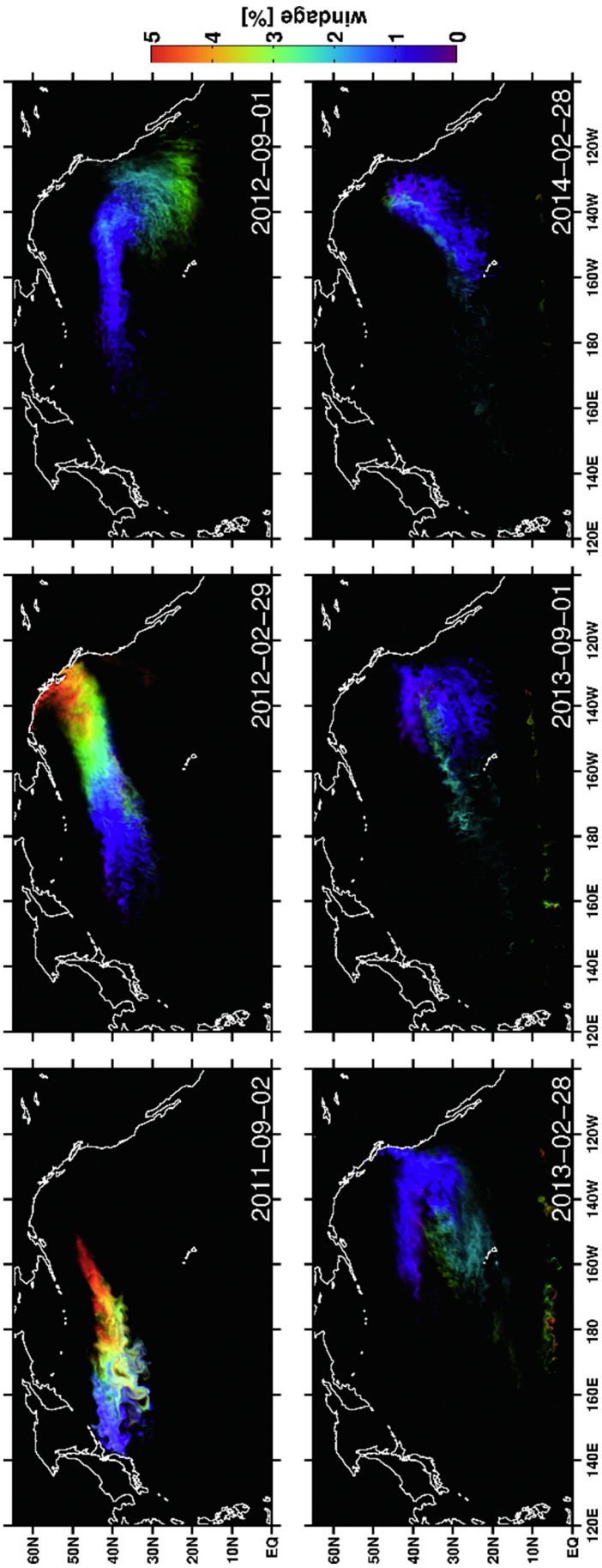

Fig. 4. Same as Fig. 2 but for the SCUD-HYCOM model simulations.

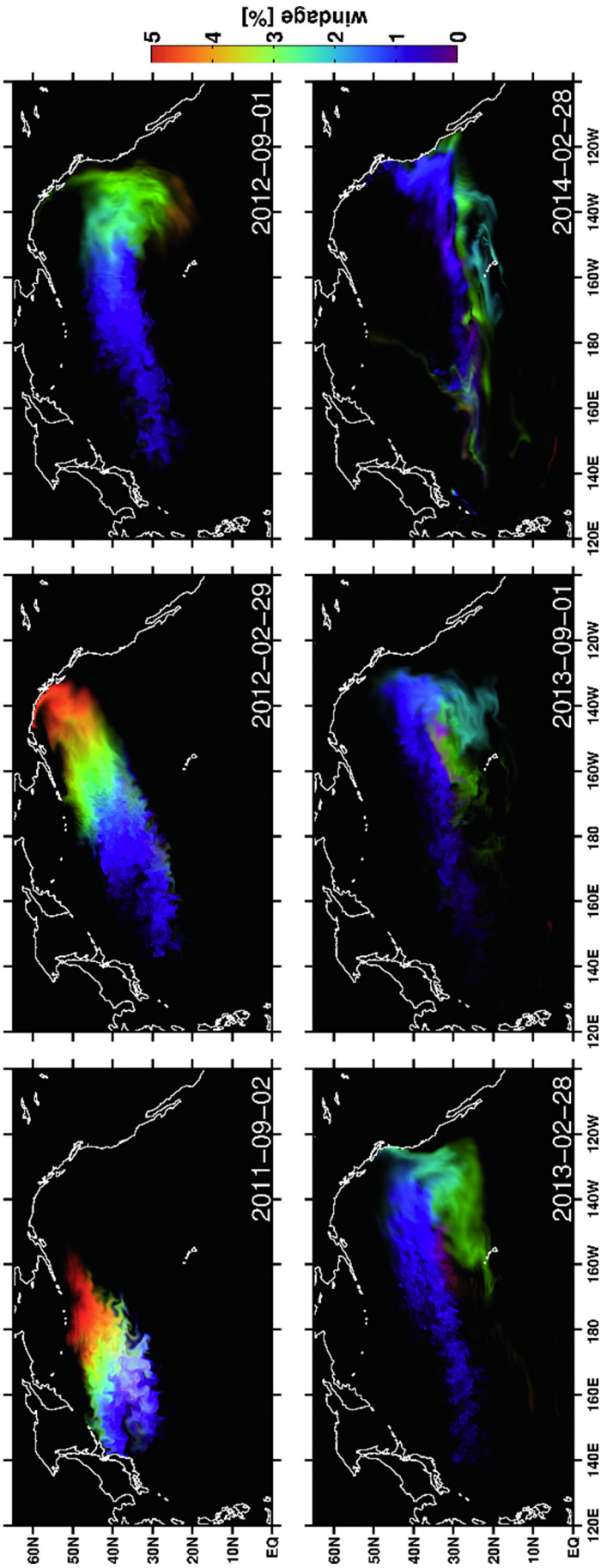

Fig. 5. Same as in Fig. 2 but for the MOVE model simulations.

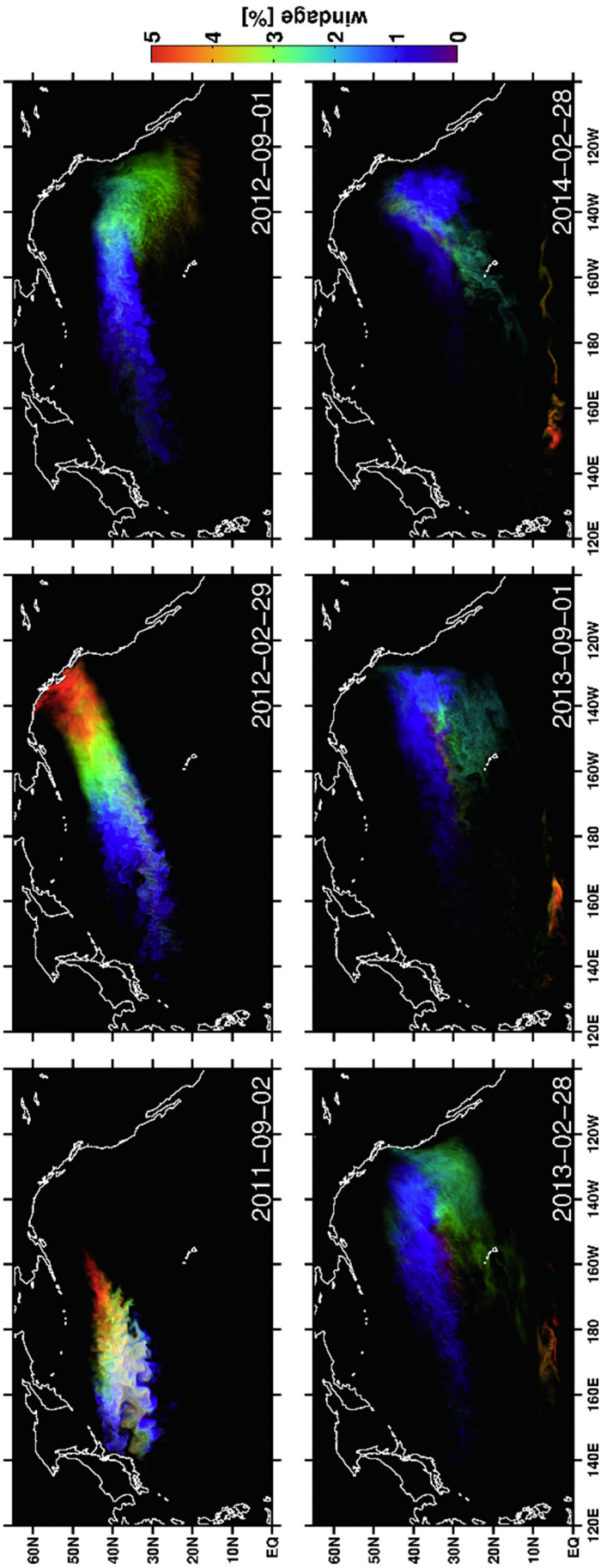

Fig. 6. Same as Fig. 2 but for the FORA model simulations.

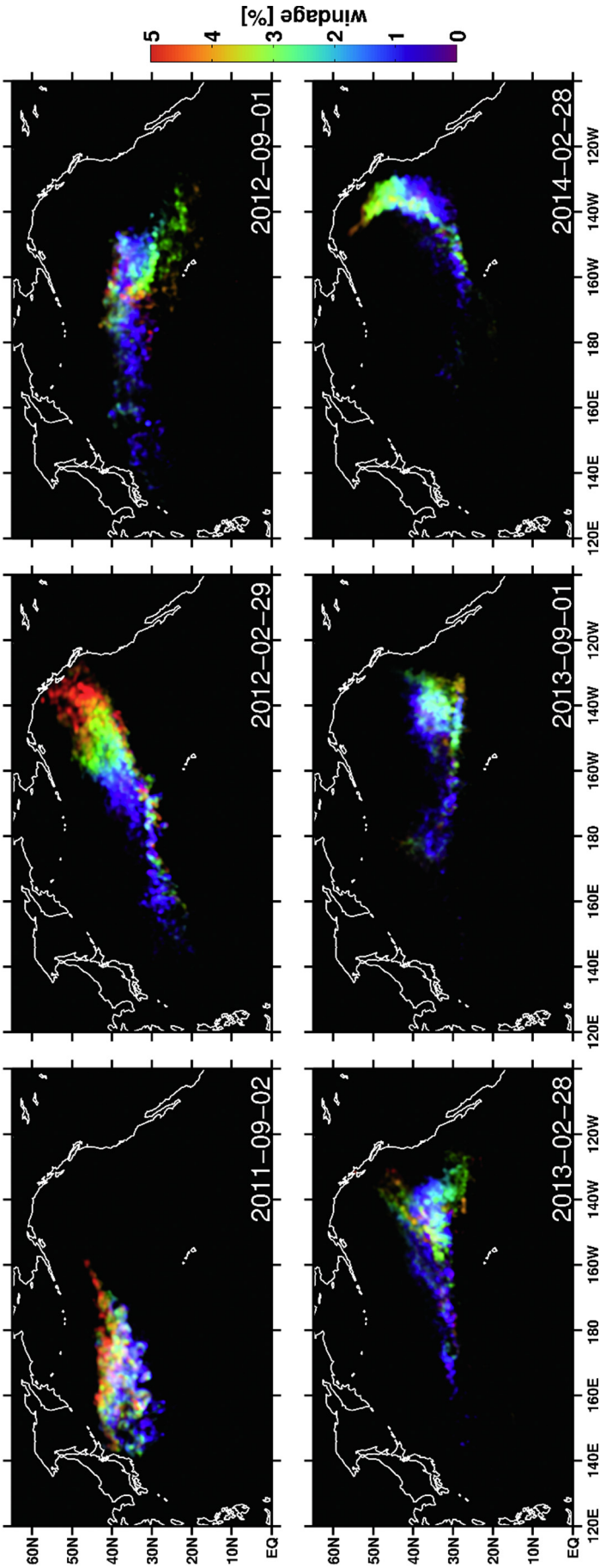

Fig. 7. Same as Fig. 2 but for the GNOME model simulations.

of the MOVE solution degrades quickly after Sumer 2013 when the model is switched to forecast mode.

Overall the agreement between FORA (Fig. 6), SCUD (Fig. 3), and SCUD-HYCOM (Fig. 4) is good. The most obvious difference is greater density of medium-windage tracer in the garbage patch in FORA than in SCUD. As mentioned before, this difference is likely due to the difference in the "surface current" definition in the two models. In practical applications, this means that the same type of JTMD has higher windage in FORA than in SCUD.

The GNOME solution in Fig. 7 differs the most from the other models. Partly, this may be due to differences between the methods based on particle trajectories and tracer concentration. Although numerical implementations may introduce important differences, the underlying equations in both methods are equivalent so that the correspondence between the particle and tracer solutions, based on the same currents and wind, should be straightforward. To facilitate visual comparison, GNOME particle distributions were converted into tracer concentrations (as described above) and plotted in the same manner as in the other four models.

As in the other models, after initialization GNOME particles drift eastward (September 2, 2011, map in Fig. 7), become stratified by windage, reach North America (February 29, 2012), and then either recirculate toward Hawaii (September 1, 2012) or collect in the garbage patch. In spite of these similarities, the structure of the GNOME solution is more heterogeneous than in the other models. For example, within relatively small areas of high particle concentration there are gaps without particles; also some regions have a mixture of particles with different windages. This heterogeneity cannot be explained by an insufficient "random walk" of particles in GNOME runs because SCUD-HYCOM and FORA also have weak numerical mixing. However, in the latter models, ocean eddies seem to amplify mixing more than in GNOME. Indeed, Douglass and Ngodock (2016) demonstrated that in HYCOM the movement of mesoscale eddies is unrealistic, although it is unclear how this would affect eddy ability to mix the ocean. The reduced mixing in GNOME is also suggested by a smaller tracer cloud in the garbage patch and alignment of particles along filaments near 30°N, reaching thousands of miles in length (February 28 and September 9, 2013). The model simulations are described further in the following section, in which their solutions are compared with observations.

4. Comparison with observational reports

In this section we compare model solutions with reports of JTMD boats. Calibrated model solutions are used in the following sections to estimate the total initial number of the boats lost in the Great Japan Tsunami and to discuss the rate of their decay.

4.1. Data description

Model solutions (Figs. 3–7) suggest that different types of JTMD are sensitive to windage, which not only affects their velocity but also their paths. Given the limited observations, we focus in this study only on reports of boats, skiffs, and small vessels lost in the tsunami. In many cases, the registration numbers were clearly visible, so that the boats could be confirmed as lost in the tsunami. This choice narrows the hydrodynamic characteristics (windage) of the debris studied. Also, unlike many other types of JTMD, the design and materials typical of these boats keep them afloat even after severe damage and/or massive biofouling. The exceptional buoyancy of the boats allows us to disregard sinks other than shorelines in our numerical experiments.

For this study several databases were tapped:

i) The debris survey[8] in NAVAREA XI (the area in the western North Pacific west of the dateline and south of 45°N), publicly available from the Japan Prime Minister's Cabinet, Headquarters for Ocean Policy (HOP). The data was collected from April to December 2011 and provided valuable information about the initial eastward drift of JTMD.

ii) The NOAA Disaster Debris (NOAA-DD) reports collected from sources in the US and Canada, including at-sea detections. This set is currently the largest coherent collection of JTMD reports and is available on request. In this publication we use the version updated on January 4, 2017.

iii) Records of JTMD removal efforts from shorelines of the Hawaiian Islands and surrounding ocean waters led by the Hawaii State Division of Aquatic Resources, Department of Land and Natural Resources (DLNR). Most of the DLNR reports were also copied into the NOAA-DD dataset.

iv) The International Pacific Research Center (IPRC), University of Hawaii, collection of JTMD reports of JTMD sightings by volunteers and partners. The IPRC team collected the data to improve its models and to simulate JTMD impacts on the Hawaiian Islands. With help of partners, the IPRC team obtained in September 2011 the first evidence of JTMD approaching Midway Island[9] and organized in Fall 2011 an expedition to monitor the debris field west of Midway.[10] Most of the reports collected by the IPRC team are also included in NOAA-DD.

The occasional reports of boats from shorelines and traced back to derelict boats belonging to local fishermen or other local people were excluded from the dataset (see Moy et al., 2017-in this issue). In other instances, we assumed that boats, whose origin was not identified, were JTMD and were kept in the dataset. There are also confirmed reports of boats lost in the tsunami sighted near Japan but these reports are sparse and not well documented, and are thus not included in our study.

After elimination of duplicates, the merged quality-controlled dataset included 327 reports: 132 from the open ocean, 104 from North America, and 91 from Hawaii. The distribution of reports among years and regions is shown in Table 1 and the geographical location and timing of reports is shown in Fig. 8. The general shift of reports of boat sightings from the western Pacific in 2011 to the eastern in 2012–2013 is evident, followed by a shift to the southwest and finally scattering over large areas in 2013–2014. These trends are illustrated by the movement of the "center of mass" of the sighting reports (gray line) and corresponding standard deviation ellipses added in Fig. 8. Consistent with model solutions (Figs. 3 to 7), in the first four months after the tsunami (purple dots in Fig. 8), boat sightings were dispersed over a large area. The first reports from North America came in the first half of 2012 and from Hawaii in the second half of 2012, consistent with model solutions for the medium-windage tracer.

4.2. Model-data comparison at sea

The pattern of reports of JTMD from the ocean shown in Fig. 8 reflects both the presence of JTMD and the availability of observers. For instance, the absence of reports from high latitudes and along the dateline is likely due to gaps in the observational network as well as bad weather conditions, especially in winter, complicating observations. Because of the unknown distribution of motivated observers, inaccessible coastlines, and the lack of negative reports (i.e. reports on the areas free from debris at the time of survey), observational data may be revealing only a part of the JTMD flow-pattern and their interpretation may be biased, preventing a complete comparison between observations and model solutions.

[8] http://www.kantei.go.jp/jp/singi/kaiyou/hyouryuu/senpaku.html.

[9] http://iprc.soest.hawaii.edu/news/press_releases/2011/pallada_tsunami_debris.pdf.

[10] http://iprc.soest.hawaii.edu/news/press_releases/2012/12_01_Tsunami_Debris_Tracking.pdf

Table 1
Number of Japan tsunami marine debris boat reports in the merged database.

	2011	2012	2013	2014	2015	2016	Total
At sea	64	28	13	14	6	7	132
North America (Stretch between 40 and 51°N)	0(0)	16(13)	31(30)	35(32)	12(9)	10(8)	104(92)
Hawaii	0	5	18	23	31	14	91
Total	64	49	62	72	49	31	327

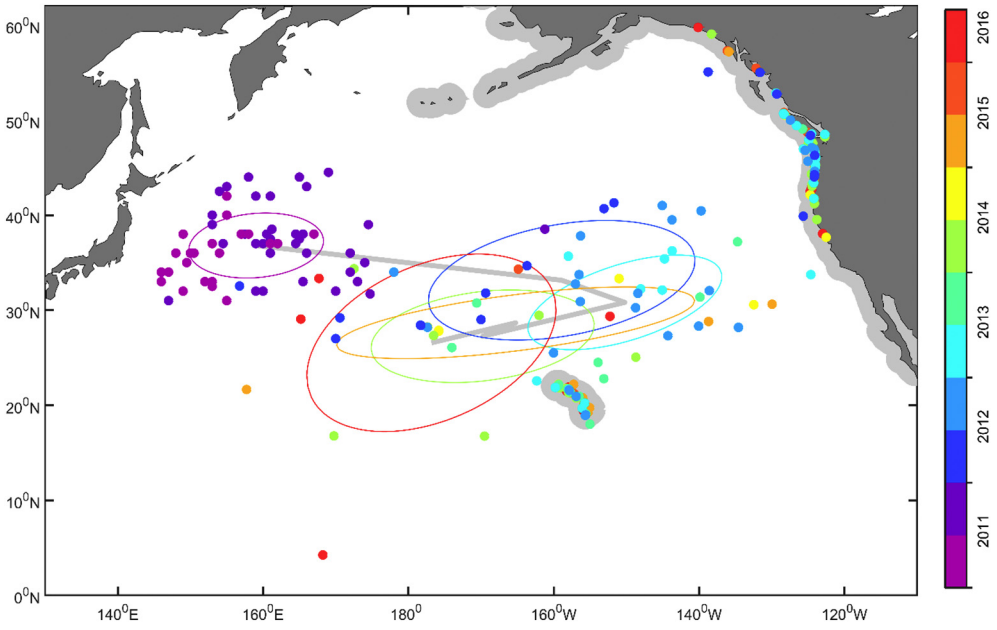

Fig. 8. Locations (dots) and years (colors) of 327 JTMD boat reports. Earlier reports are plotted on top of later reports. Gray line connects mean positions of annual "at sea" reports (total 132). Colors of standard deviation ellipses correspond to the *year for which they are calculated*. *Coastal* areas in North America and Hawaii are masked by a gray background. Distribution of reports over different regions and year is described in Table 1.

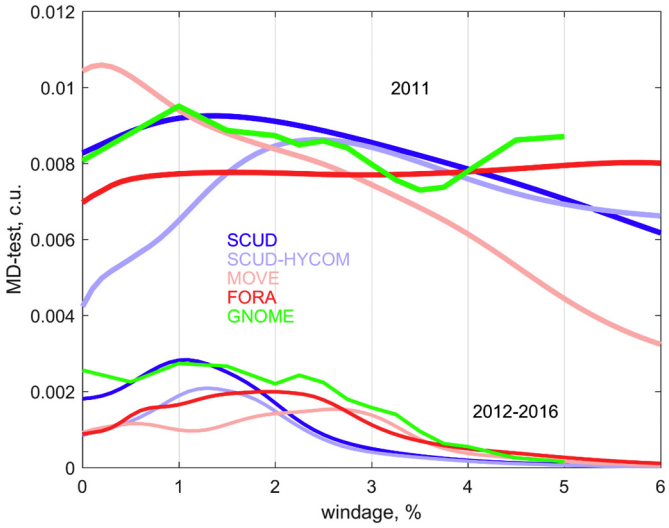

Fig. 9. Results of the MD-test, described in the text, for five models as a function of windage parameter. Upper group of thicker lines integrates model solutions over at-sea data collected during 2011 (reports before May 16, 2011 are excluded). Lower group of thinner lines is for integration over 2012–2016. Only the hindcast part of the MOVE model solution (through July 1, 2013) is taken into consideration.

In this study we developed a new procedure, called hereafter the "model-data-test" or "MD-test," that allows quantitative comparisons among different model runs with fragmentary observations. The procedure is based on the implicit assumption that density of available observers is not correlated with the density of JTMD. In this case, model performance can be characterized by the summation of the tracer probability density function (PDF) sampled at times and locations of actual reports, where the PDF is calculated from the model tracer concentration by normalizing the latter with the total amount of tracer initially released:

$$\mathrm{MD} = \sum_i PDF(x_i, y_i, t_i), \tag{1}$$

where

$$PDF\ (\mathrm{x}, \mathrm{y}, \mathrm{t}) = C\ (\mathrm{x}, \mathrm{y}, \mathrm{t}) / \iint C(x, y, 0)\,dx\,dy, \tag{2}$$

C is tracer concentration, x, y, t are longitude, latitude, and time, respectively, and summation is over individual reports i.

In other words, the more observational reports coincide with a high model PDF, the higher the MD values. It is important to emphasize that the method accounts not only for the spatial pattern but also for the temporal evolution of the JTMD field, i.e. not only the places that were visited by JTMD were evaluated but also the timing of these visits. The method's limitation is that it is biased toward regions with high density of reports and works best if observational surveys coincide with the highest concentration of the JTMD field. However, the same limitation is common to all other methods we know, including visual comparison.

Because there is a lot of vessel traffic in an area, doesn't mean there will be a lot of observations (regardless if debris is present). This can be illustrated with by the example of the front associated with the North Pacific Current, in which fisheries are very active and which the tracer crossed in all model solutions in 2011–2012 (Figs. 3 to 7). The number of reports from fishing ships working in the area is surprisingly small and may be explained by a lack of motivation.

The MD-test was applied to solutions of the five models for different values of windage (Fig. 9). Only at-sea reports, shown in Fig. 8 outside of the gray masked areas (located more than 90 nautical miles from any shore), were used for this analysis. Because nearly half of the reports (64 out of 132, Table 1) were in Year 2011 and because the concentration of model tracer decays with time, contributions to MD from year 2012 to 2016 (Eq. (1)) are much smaller than from 2011. However, analyses of these later years may yield more information than the analysis of 2011. Indeed, the early evolution of the JTMD tracer field may be imprecise as it depends more strongly upon the distribution of

JTMD sources along the Japan coastline, which is not well known and not reproduced in the models, and on the near-shore currents, which remain a challenge for ocean circulation model simulations. Dispersion of JTMD with time increases the spatial scale of the pattern, making both surveying and modeling more accurate. Fig. 9 shows the MD-test results separately for reports collected in 2011 (group of lines with the larger MD values) and from 2012 to 2016 (smaller MD values). In these calculations we ignored the five reports before May 16, 2011, because before then some model solutions still show "blobs" of high tracer concentration reflecting model setups, which coupled with single or few reports results in misleadingly high MD values.

The MD-tests based on the 2011 reports are generally inconclusive (Fig. 9). Only SCUD and SCUD-HYCOM models demonstrate a single-peak structure with maxima at 1.3% and 2.5% windage, respectively. MD values for the MOVE model monotonically decrease and for FORA increase with windage. GNOME MD shows the highest peak at 1% and a second, lower peak at 5% windage.

The results of the MD-tests for 2012 to 2016 are much more informative; the highest MD values are for intermediate windages in all models. MD peaks at 1.1% for SCUD, 1.3% for SCUD-HYCOM, and 2.1% for FORA (Table 2). The profile of MD for MOVE is broader, with a shallow peak at 2.8%, perhaps due to the small size of the data subset overlapping with the hindcast period (only 18 months). The MD values in GNOME vary more than in the other models, probably because particle-based models tend to simulate patchier flows than tracer-based models as previously discussed (Figs. 3 to 7). After smoothing along windage, the GNOME MD has a relatively flat maximum between 1.0% and 1.5%. These maxima of MD provide the first estimates of optimal windage for JTMD boat drift simulations.

The MD peak values are similar in SCUD and GNOME, and somewhat lower in SCUD-HYCOM, MOVE, and FORA. Since these differences can be explained by intrinsic differences between the models, we see that, overall, the 5 models reasonably simulate the JTMD boat reports from the open ocean. The lower MD values in SCUD-HYCOM and FORA can be explained by the fact that in these two models large fractions of tracer (up to 25%) are washed back to Japan in the first weeks of the simulations. The lower MD values in MOVE are explained by the short time span of the model runs.

4.3. Model-data comparison on the US/Canada West Coast

There was a high density of JTMD boat reports along the North America shoreline, comprising 104 reports (Fig. 8). Of these reports, 92 were received from the US/Canada West Coast (WC) between 40°N (Northern California) and 51°N (northern tip of Vancouver Island); their locations are mapped in Fig. 10a. Monthly numbers of reports (blue bars in Fig. 10b) reveal three main peaks (July 2012, March 2013, and May 2014) and two secondary peaks (April 2015 and April 2016). Conversion of discrete data into a continuous timeline (black line in Fig. 10b) by smoothing with a Gaussian filter of 1.5-month half-width suggests one additional small peak in October 2013. Four out of the six peaks occur in the spring, between March and May, suggesting that local seasonality affects the inflow of floating matter on the WC (see Kako et al., 2018). This seasonality of the inflow is consistent with the "Aleutian low" affecting North Pacific weather in late winter – early spring and the "subtropical high" in summer and fall. As a result, during winter the westerlies associated with the "jet stream" are stronger than usual, whereas during the summer, winds are anticyclonic, strengthening in the upper ocean the convergence of surface currents toward the garbage patch, the area of the convergence corresponding to accumulation of low-windage model tracer shown in the maps at the end of the simulations (Figs. 3 to 7).

Peaks in JTMD boat observations in July 2012 and October 2013 occur outside the "season" and the magnitudes of the peaks vary in a complex way that indicate that other processes, including interannual variability of the ocean-atmosphere system, also play important roles. Also, mean currents and winds are strong in the North Pacific (e.g., Maximenko et al., 2009) and they move the tracer around the basin (Figs. 3–7) with Lagrangian time scales not synchronized with the seasons.

Analysis of WC JTMD data reports shows that, with all the complexity of the timeline (Fig. 10b), the reports came in waves from all latitudes (Fig. 10c). This coherence fits a simplified conceptual model in which JTMD is driven by the large-scale ocean and atmosphere dynamics and the WC acts as a "wall." When favorable conditions are present for several months, JTMD floating offshore is pressed against this wall and washes up on beaches. This model justifies inclusion of several reports on JTMD boats not from the shoreline but floating close (within 90 nautical miles) to the WC.

The coherence of JTMD flux at different latitudes justifies combining the reports from a 1200-km-stretch along WC shorelines into a single timeline. However, Fig. 10d shows that the flux of JTMD was not distributed uniformly along the shore: the number of reports was higher between 44°N and 48°N than north or south of this latitude band.

To compare with observations, model tracer fluxes from the ocean into the coastal bins were processed in a manner similar to that applied to the data in Fig. 10b: i.e., tracer and particles "washing" up on the model WC were integrated for every time step and for every windage between 40°N and 51°N. Time-windage diagrams of the integrated fluxes are shown in Fig. 11a–e, which reveal several time scales. Narrow vertical bands evident in the figure reflect weather events from a few days to a few weeks in duration during which the flux increases for all windages. This high-frequency variability is modulated by a low-frequency signal that becomes clearer after application of a low-pass Gaussian filter with a 1.5-month half-width (same filter that was used on the observational data). Fig. 11f–j show complex patterns of events of various magnitudes associated with greater influxes that last for several months and occur at different times for different windages.

High-windage tracer in the models arrives on the WC before low-windage tracer (Figs. 3 to 7), which is also seen clearly in the fluxes in Fig. 11a–e. The dashed white line in Fig. 11d marks the "forefront" of the JTMD influx to the WC in FORA. Similar fronts are present in the diagrams of the other models (less clear in GNOME in Fig. 11e). Comparison of the arrival times for different windages in different models suggests that increasing windages by 0.5%–1% in SCUD and SCUD-HYCOM results in fluxes most similar to those in MOVE or FORA. A similar conclusion is reached in Section 3 when comparing Figs. 3 to 6. Again, GNOME differs from the other models in its fluxes (Fig. 11e

Table 2
Optimal model windages and best fits in at-sea and West Coast analyses.

	MD-test (2012–2016)	Single optimal windage		Optimal windage range		Ensemble of windages: relative rms error
		Windage value	Relative rms error	Windage range	Relative rms error	
SCUD	1.1%	1.7%	0.56	0–2.1%	0.51	0.36
SCUD-HYCOM	1.3%	1.9%	0.55	0.4–0.7%	0.53	0.37
MOVE	2.1%	1.8%	0.37	1.6–2.0%	0.37	0.14
FORA	2.8%	1.5%	0.55	1.0–1.9%	0.53	0.46
GNOME	1.0–1.5%	1.5%	0.73	1.5–1.5%	0.73	0.71

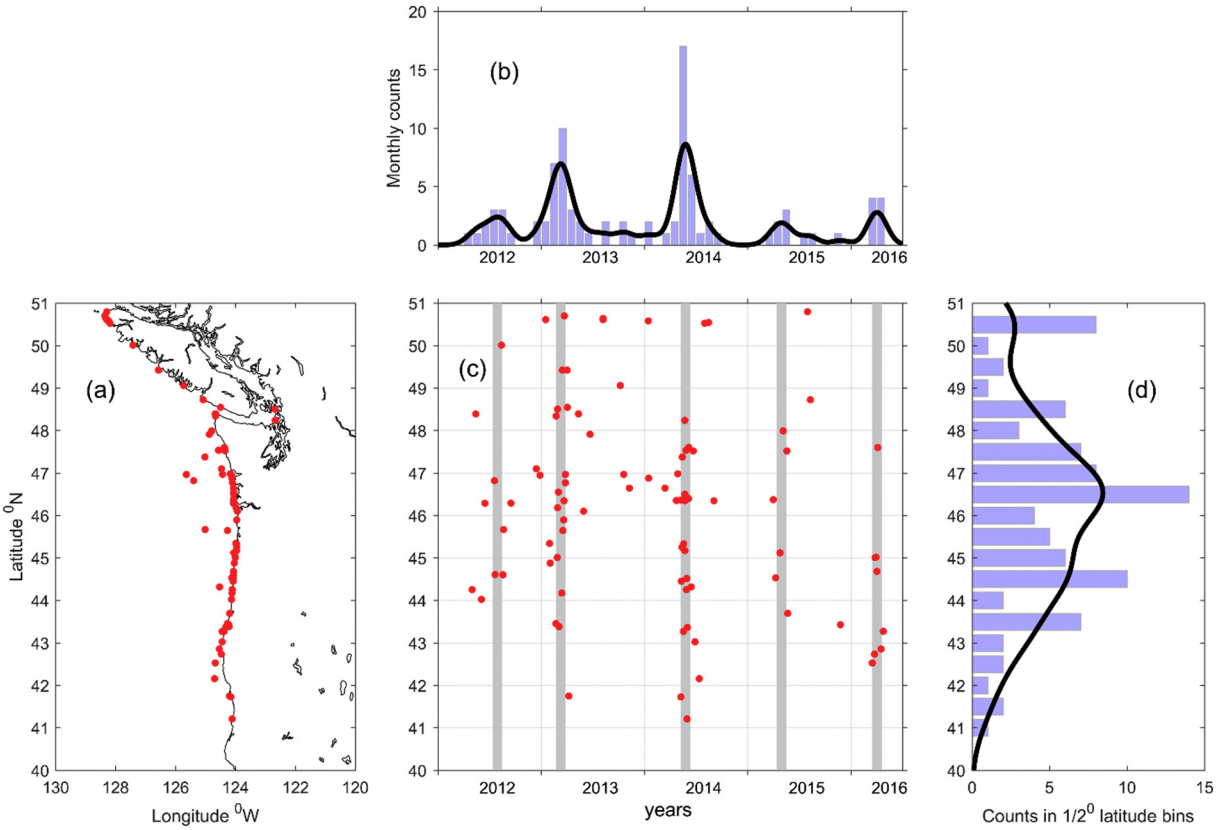

Fig. 10. Time-space distribution of 92 boat reports from and near the 40–51°N stretch of the North America west coast. (a) Location of report (red dots) on the map. (b) Monthly timeline of reports (blue bars) and result of smoothing with a Gaussian filter of 1.5-month half-width (black line). (c) Time-latitude diagram of reports (red dots). Gray lines mark times of five main peaks in (b). (d) Distribution of reports with latitude: blue bars denote number of reports in ½-degree latitude bins and black line is the result of smoothing with a Gaussian filter of 1° half-width. (For interpretation of the references to color in this figure legend, the reader is referred to the web version of this article.)

and j), having fewer and sporadic peaks that occur at about the same time periods over a broad range of windages.

After 2012, the greatest fluxes are found at intermediate windages. This is because much of the high-windage tracer is withdrawn from the ocean during the first wave of landings and the low-windage tracer drifts into the garbage patch where it tends to stay in the converging currents.

The model solutions generate multiple peaks in fluxes, marked in Fig. 11f–j with white dots and lines. The timing of these peaks is sensitive to windage in 2012 and 2013 but becomes less so from 2014 to 2016. Each peak in the reports (vertical magenta lines in Fig. 11f–j) occurs close in time to at least one peak in the model fluxes. The exception is GNOME, in which the first model peak leads the first observed peak in July 2012 by several months for all windages. However, it is unclear how well the models can reproduce the observed peaks with a single windage value or a set of windages. To investigate this correspondence between the models and observations, we scaled model fluxes using a regression coefficient A, calculated as

$$A(w) = \int F(t,w) * Obs(t)\,dt \Big/ \int F(t,w)^2\,dt, \tag{3}$$

where F is the model flux on the WC (Fig. 11f–j), Obs is observational flux (Fig. 10b), t is time and w is windage. The relative root-mean-square (rms) error between the observational data and scaled model flux was calculated as follows:

$$D(w) = sqrt\left(\int (F(t,w) * A(w) - Obs(t))^2 dt \Big/ \int Obs(t)^2 dt \right) \tag{4}$$

The time periods used in fitting the data (Eqs. (3) and (4)) were synchronized with the time span of the model solutions and are shown with horizontal gray lines in Fig. 11f–j. They all start on March 11, 2011 and end as follows: July 1, 2013 for MOVE, end of 2015 for FORA, and end of 2016 for SCUD, SCUD-HYCOM and GNOME.

The misfit, D, between the number of boat-sighting reports and tracer density at different points in time in the different models depends on the windage as shown in Fig. 12; windage values yielding the best fit are shown in Table 2. The smallest rms error (0.37) between model solutions and observed reports occurs with MOVE at 1.8% windage. This is not surprising because the MOVE solution spans a rather short period with the two observed peaks (Fig. 11h). The best fit (0.55–0.56) between observations and SCUD, SCUD-HYCOM, and FORA fluxes is obtained at 1.7%, 1.9%, and 1.5% windage, respectively. The best fit for the GNOME fluxes is broad and shallow (with the low rms error ranging between 0.5% and 3.25% windages), with the best fit of 0.73 at 1.5% windage. The optimal windages are marked in Fig. 11f–j with gray horizontal lines.

The optimally scaled model fluxes for these windages are shown in Fig. 13a together with the observational timeline (black line). Two models, SCUD (deep blue) and SCUD-HYCOM (light blue), capture all six peaks (three main, two secondary, and one additional) described in the beginning of this section. Although not perfect, the overall similarities between the peak magnitudes in these models and observations are striking. The first two peaks in the models occur two to three months earlier than in observations. This lag may be due to the delays between boat arrival, detection, and reporting before the reporting system was well established.

The optimal FORA solution (deep red) captures the second and third main peaks but misses the others. Also, contrary to observations, the first peak is higher than the second peak. (SCUD and SCUD-HYCOM also have this problem.) The MOVE solution (light red) successfully reproduces the second peak while missing the first peak completely.

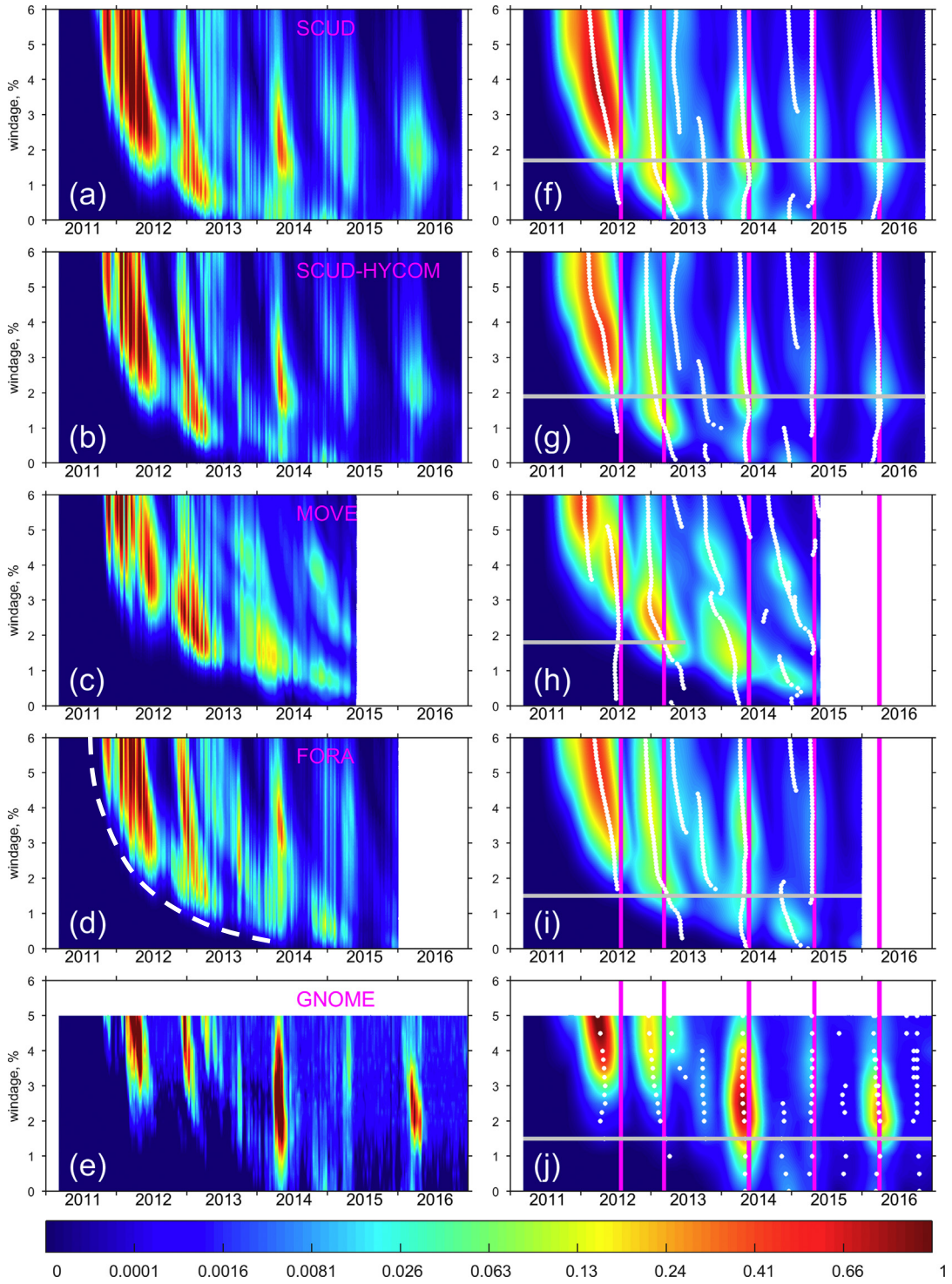

Fig. 11. Model fluxes on the North America west coast between 40 and 51°N, shown in Fig. 9a. Rows (from top to bottom) correspond to SCUD (a and f), SCUD-HYCOM (b and g), MOVE (c and h), FORA (d and i), and GNOME (e and j) models. Left column shows original model fluxes and right column same fluxes smoothed in time with a Gaussian filter of 1.5-month half-width. White dots and lines mark peaks in model fluxes for different windages. Vertical magenta lines mark five main peaks in observations (Fig. 9b and c). Horizontal gray lines mark the optimal windage parameter values, derived from model comparison with boat reports, and span over the periods of the comparison. Color scale is strongly nonlinear and model flux units are fraction of the released tracer per year. White dashed line in (d) illustrates faster drift and earlier arrival of higher windages. (For interpretation of the references to color in this figure legend, the reader is referred to the web version of this article.)

Moreover, the third peak in MOVE (dotted line; February 2014) leads the third reported peak (May 2014) by 3 months.

The GNOME solution (green line) also captures only two peaks: the third main peak in 2014 and the last, smaller peak in 2016. Fig. 11j suggests the traces of the first and second peaks may be present in model fluxes at high (4%–5%) windages but both model peaks lead observations by 3–4 months.

In reality, the windage of individual JTMD boats varies because of their design, the damage incurred during the tsunami, the amount of biofouling, and their orientation in the water. Photos in Fig. 14

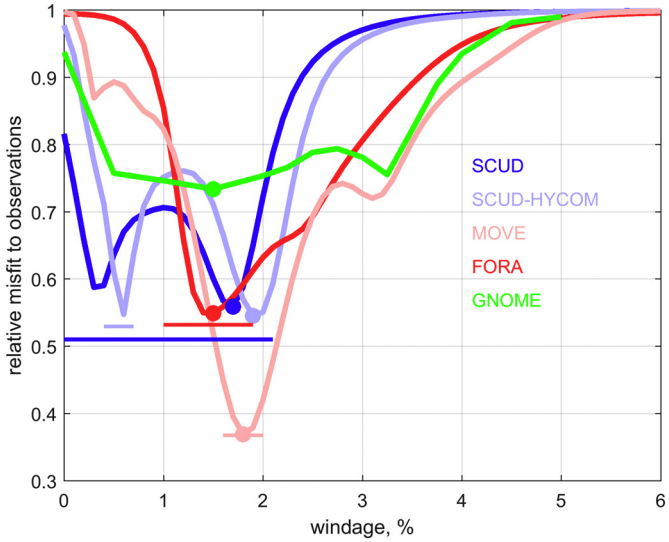

Fig. 12. Relative r.m.s. misfit of optimally scaled model solutions to WC boat observations for different windages. Filled circles mark the best fit. Four horizontal lines show the optimal range of windages and minimum misfit as described in the text and in Fig. 14 for SCUD, SCUD-HYCOM, MOVE, and FORA. For GNOME range optimization coincides with the single-windage case.

illustrate that boats could float not only upright or upside down but also vertically or partially submerged. Model solutions suggest that boats drifting under different windages may have somewhat different paths and destinations. Higher-windage boats are expected to be more frequent in reports from shorelines, while lower-windage boats are expected to be seen more often in at-sea reports. Possibly, this explains the lower optimal windages in SCUD and SCUD-HYCOM, derived from the MD-test (1.1% and 1.3%, respectively), than from the West Coast (1.7% and 1.9%).

To consider the effects of multi-windage composition, we used the technique similar to the one described by Eqs. (3) and (4) except that the tracer source was distributed uniformly within a range of windages. Fig. 15 shows the relative rms misfit between model solutions and West Coast reports for all possible windages. Note that the there is a strange pattern of vertical contours in Fig. 15c at windages below 1.5% because these windages in the MOVE solution do not reach the WC during the hindcast phase of the model, ending July 1, 2013. The best fit and the windage ranges at which they occur are listed in Table 2 and visualized in Fig. 12. Fig. 13b shows the new timelines of optimized fluxes.

MOVE and FORA simulations improve slightly from broadening the windage range 1.6%–2.0% and between 1.0% and 1.9%, respectively. The GNOME simulation, on the other hand, shows the best fits with reports at a single-windage (1.5%) solution. The biggest changes are in SCUD and, especially, in SCUD-HYCOM. The numbers of reproduced peaks in fluxes remain the same in these models as in the single-windage case (Fig. 13a). In SCUD, the mixture of tracers with windages between 0% and 2.1% reduces the rms error to 0.51 (from 0.56 for the single 1.7% windage). The new timeline of SCUD fluxes again successfully reproduces six observed peaks. The differences from the single-optimal-windage timeline are small and mainly associated with the adjustment of the peak magnitudes.

The biggest changes with multi-windage composition are in SCUD-HYCOM. Fig. 12 shows that the formal errors are the smallest for two windage values, with the misfit for 0.6% windage being only slightly larger than one for 1.9% windage. The cause of the two "optimal" windages is currently not known and the timelines for these windages are very different. While the windage mixture in the range between 0.4% and 0.7% provides a slightly smaller error (0.53 compared to 0.55 for a single 1.9% windage), the new SCUD-HYCOM timeline in Fig. 13b misses the first main peak in 2012 and a secondary peak in 2015. Moreover, the solution shows a small peak in the end of 2014 not seen in observational reports. Fig. 15b shows a peak in the rms error around the 1% windage, surrounded by lower errors at lower and higher windages. Fig. 11g shows that model fluxes during the observational peak in May 2014 are minimum for this 1% windage, resulting in higher errors of model-data regression. SCUD fluxes demonstrate (Fig. 15a) a similar error pattern but switching from a single-windage case to a windage-range does not degrade reproduction of most of the observed peaks.

The misfit between the models and observations can be significantly reduced using more complex combinations of windages. For example, with the linear combination of all windages for SCUD, the misfit becomes as small as 0.20. This case, however, is unrealistic because for some windages, tracer fluxes take negative values, the coefficients oscillate between positive and negative values for adjacent windage values and the "optimized" model fluxes are very noisy. In part, this is because the model fluxes at close windages are correlated and together do not form an "orthogonal basis".

Interesting results have been obtained by allowing all windages but forbidding negative fluxes. Analytical solutions of this mathematical problem possibility do not exist and, at least theoretically, multiple optima are possible. The iterative process used in this study was based on adjusting one windage at a time to regress the difference between the observations and the optimal model signal from the previous step. The coefficients for individual fluxes were not allowed to become negative, and iterations stopped when all positive options were exhausted. To ensure that the best possible fit is obtained, the calculations were repeated multiple times from randomly selected initial conditions. The differences between these experiments were surprisingly small, so that we are confident that we detected the best fits, although we cannot prove this analytically.

Fig. 16 shows the relative magnitudes of model fluxes, scaled using the described method and converted into a fraction of tracer influx on the West Coast. The rms errors are shown in Table 2. While we expected that coefficients of windages will group around one most probable value, remarkably, all five models fit observations best as a combination of two windage ranges: 0.3%–0.6% and 1.7%–1.8% for SCUD; 0.4%–0.7% and 2.0%–2.1% for SCUD-HYCOM; 1.7%– 1.8% and 3.5%–3.6% for MOVE; 1.3%–1.4% and 2.8 for FORA% and 1.5% and 3.5–4.0% for GNOME.

More research is needed to understand whether these results with two model-preferred windages for JTMD boats are realistic (e.g., high-windage for the boats drifting in the upright position and low-windage for all other orientations), or if more complex scenarios (such as windage changes with time) should be studied. The higher values of the pairs of preferred windages in MOVE and FORA compared with SCUD and SCUD-HYCOM are again consistent with the discussion in previous sections.

Inclusion of more windages improves comparison with reports from the West Coast (Fig. 13c). MOVE now reproduces two peaks with an rms error as small as 0.14. FORA reproduces five out of six peaks (0.46). With a small reduction in the rms error to 0.71, GNOME now shows two early peaks (years 2012 and 2013), leading by 3–4 months those in observations, the second peak being smaller in GNOME. In SCUD and SCUD-HYCOM the rms errors of the individual peaks decrease (0.36 and 0.37, respectively) but results in a poorer fit of the model solutions with the April 2015 peak. In all models (except MOVE which ends before that time), this peak is still seen as a small bump in the tail of the higher peak at the end of 2014, which is not supported by observations.

The majority of the JTMD boat reports came from the central part of our West Coast domain (black lines in Figs. 10d and 16), and fewer from central and southern California and Alaska (Fig. 8). We believe that this pattern reflects the actual JTMD flow, though the results could be affected by accessibility and recreational use of the different coastlines as well as by local dynamics of the near-shore circulation. The histogram in Fig. 10d shows five regional peaks, each associated with a

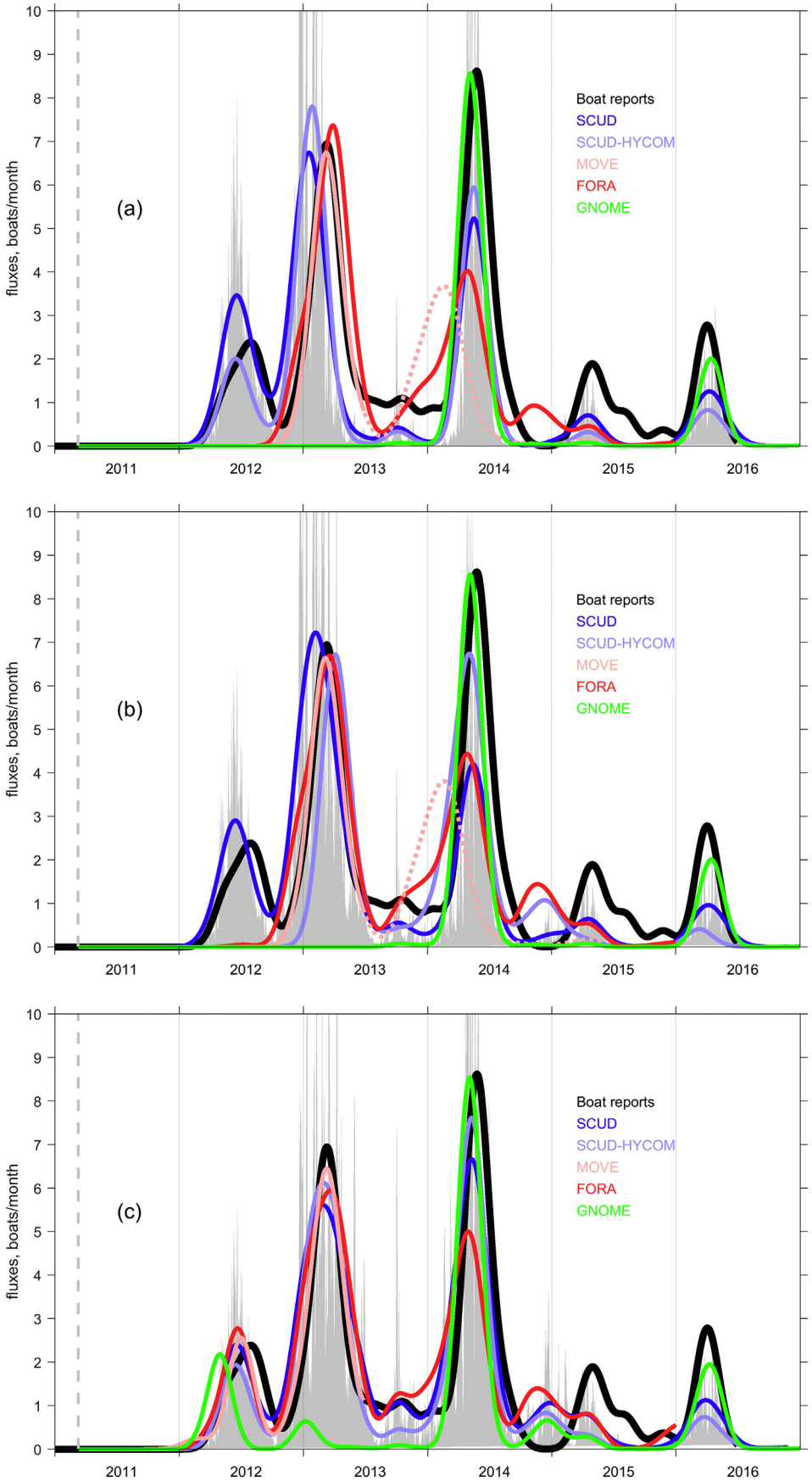

Fig. 13. JTMD boat observations (black line) and scaled model fluxes on the North America west coast for (a) single windage parameter values, minimizing misfit shown in Fig. 11, (b) optimal range of windage parameter, minimizing misfit shown in Fig. 14, and (c) multi-windage approximation with windage distribution shown in Fig. 15. Lines present timelines, smoothed with a Gaussian filter of 1.5-month half-width. Gray background shows unsmoothed scaled SCUD solution at optimal windage. Vertical dashed gray line marks the moment of the tsunami. Units are number of boats per month.

Fig. 14. Photographs of JTMD boats, taken (left) June 27, 2012 at 34°41′ N by 163°41′ W (850 nautical miles north of Kauai Island) and (right) January 22, 2017 off Kona, Island of Hawaii.
Credits: Randall Reeves and Jeffrey Milisen.

special coastline feature (ordered from north to south): the northern and southern tips of Vancouver Island, Long Beach, Oregon (Columbia River mouth), Newport (Yaquina River), and Reedsport/Coos Bay, Oregon (Umpqua and Coos Rivers). JTMD appeared to end up on coasts at locations that are typically more polluted by marine debris from other sources, not relevant to the tsunami. The details of the shoreline and near-shore dynamics are not represented well in the basin-scale models used in this study but the distributions of on-shore fluxes smoothed by latitude (Fig. 17) still have maxima within the domain. This pattern is robust. The along-shore distributions of JTMD boat reports before July 1, 2013 (38 reports, Table 3) and after (54 reports) are similar in shape, with the exception of 8 reports from 2016 that came mostly from south of 46°N.

5. Total budget and future projections

The ability of the models to reproduce the observed timeline of JTMD boats arriving on the West Coast allows us to convert the model solutions into practical units to estimate the total number of JTMD boats set afloat by the tsunami and the probable numbers and locations of boats still in the water, and also to project the decay rate of these numbers. The critical parameter that links the observations to model tracers or particles is windage. Windage, though, is not known from direct observations and may vary between the models. Previous sections discussed the effects of windage on different JTMD pathways and the sensitivity of model simulations to hypothesized windage compositions.

By scaling model solutions for a single optimal windage (Table 2), we estimated the total number of "model boats" accumulated on the West Coast at the end of each experiment (Table 3). Knowing the relationship between these numbers and the corresponding fraction of initial model tracer (or particles) allows us to estimate the initial number of JTMD boats. These fractions, calculated at corresponding optimal windages, vary from 0.04 for FORA to 0.14 for SCUD (Fig. 18; column *iii* in Table 3). Thus, averaged over the five models, the estimated number of boats lost in the tsunami is 637 and varies from 354 for GNOME to 927 for FORA (*iv* in Table 3).

For several reasons these numbers are an underestimation. First, the regression uses only the reports that correlate best with the timeline in the optimal model solution. As a result, the numbers of boats in the model solutions are systematically lower than in actual reports, as seen by comparing columns *i* and *ii* of Table 3. If instead, the model solutions are scaled to reproduce the number of reports (at optimal windages), the average model estimates of JTMD boats at the source rises to 998, with a low of 676 for SCUD and high of 1217 for FORA. In this case, the most dramatic change is in GNOME, whose original estimate of the total at the source (354 boats) is very close to the number of reports (327) in our definitely incomplete database.

The other possible reason for underestimation is the presence of JTMD boats with windages lower than considered "optimal" in the model solution. The fraction of tracer reaching the West Coast is generally smaller for lower windages. In other words, at lower windages (Fig. 18) the same number of West Coast reports would result in higher "at-source" estimates. Our experiments with windage-ranges and multi-windage cases showed that, indeed, adding low-windage tracer may improve the correspondence between the models and the JTMD boat reports. Due to the limited number of observations, however, this possibility was not pursued.

The general consensus among the five model results is that the tsunami released approximately 1000 boats into the ocean, a number consistent with the information available from agencies in Japan. On November 16, 2011, the Japan Coast Guard detected 506 skiffs/vessels drifting off the devastated shoreline. The Ministry of Agriculture, Forestry and Fisheries (MAFF) of Japan estimated the total number of fishing skiffs/vessels lost or destroyed by the tsunami as 18,936 but how many of these vessels drifted away and how many remained on the devastated shores was unknown. The Ministry of the Environment of Japan estimated that the total tonnage of JTMD skiffs and vessels was about 102,000 tons but the total tonnage of skiffs/vessels that floated away was only 1000 tons.

The model simulations help to understand the evolution of the JTMD field. Maps in Figs. 3 to 7 show that high-windage tracer tends to wash ashore sooner than low-windage tracer. The latter tends to move into the subtropical gyre, with its highest density in the garbage patch. A fraction of tracer escapes from this patch as a result of eddy diffusion, weather events, seasonal, interannual, and other changes in the large-scale currents and winds. This prediction is not exactly in accord with the JTMD boat reports in Fig. 8, which shows that in 2015 and 2016 at-sea reports were coming from an area increasingly west of the garbage patch. This discrepancy from model solutions is likely due to a bias in the observing system; due to low biological activity, the garbage patch is avoided by fishermen and due to weak winds by sailors. This may

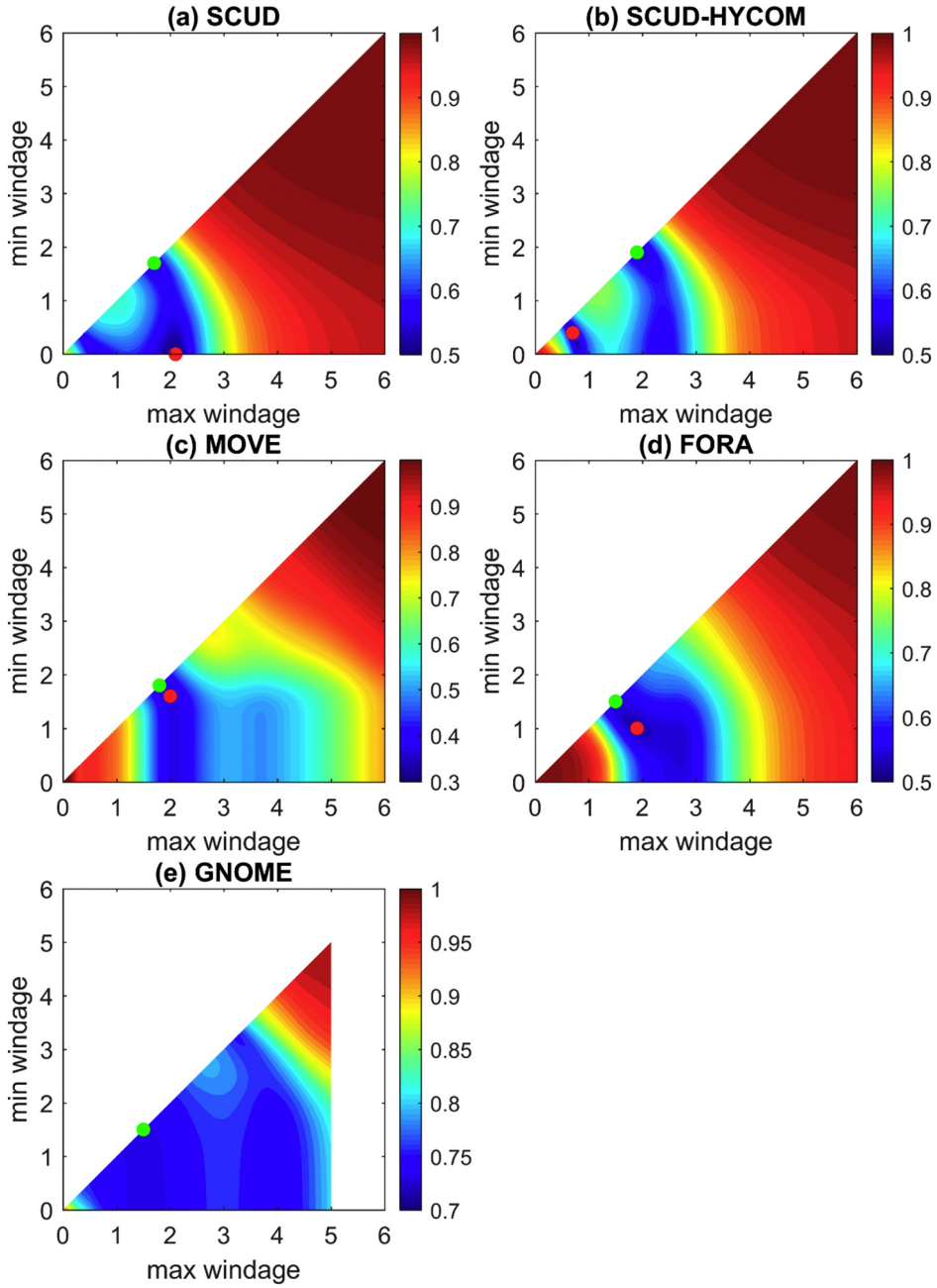

Fig. 15. Misfit between (a) SCUD, (b) SCUD-HYCOM, (c) MOVE, (d) FORA, and (e) GNOME model fluxes and JTMD boat reports on WC as a function of tracer windage ranges. The ranges are limited by minimum values on vertical axis and maximum values on horizontal axis. Windage units are per cent, misfit units are non-dimensional. Red dots mark the minimum. Green dots mark optimal windages for the single-windage case (Fig. 11). (For interpretation of the references to color in this figure legend, the reader is referred to the web version of this article.)

explain the smaller number of reports coming from the garbage patch than from east or west (at-sea and Hawaii) of the patch.

The fraction of model tracer with optimal windage remaining in the water through time is shown in Fig. 19. Under the assumption that coastlines are the only sink of JTMD boats (i.e., that their number cannot decrease as a result of sinking or breaking into small pieces) and that the climatology of ocean currents and atmospheric winds does not change significantly from one year to the next, these timelines can be used to estimate the decay rate of the JTMD signal with time. Almost all models lose significant amounts of tracer in the first months after the tsunami by washing back onto the eastern shore of Japan (Fig. 19). This initial development is difficult for the models to simulate because of the complex coastal dynamics and cannot be confirmed because of lack of observations.

In 2011–2012 each model has a period when the tracer or particles drift across the North Pacific without coming into contact with shorelines. After 2012 all models demonstrate a steady nearly exponential tracer decay with a timescale that can be determined. The *e*-folding time scales (time during which variable decrease by a factor of $e \approx 2.72$), calculated for different models, are listed in column *vi* of Table 3. Under the assumption of 1000 initial JTMD boats, 406 boats were still floating in MOVE by July 1, 2013; 564 in FORA by the end of 2015; and 300 in SCUD, 173 in SCUD-HYCOM, and 564 in GNOME by the end of 2016. The number of boats estimated still floating by the end of 2018 is as follows: 174 in SCUD, 82 in SCUD-HYCOM, 393 in FORA, and 515 in GNOME. The GNOME timeline consists of a set of 'no decay' periods, separated by sudden short periods of tracer loss that make predictions more difficult. We did not use MOVE in this calculation. All

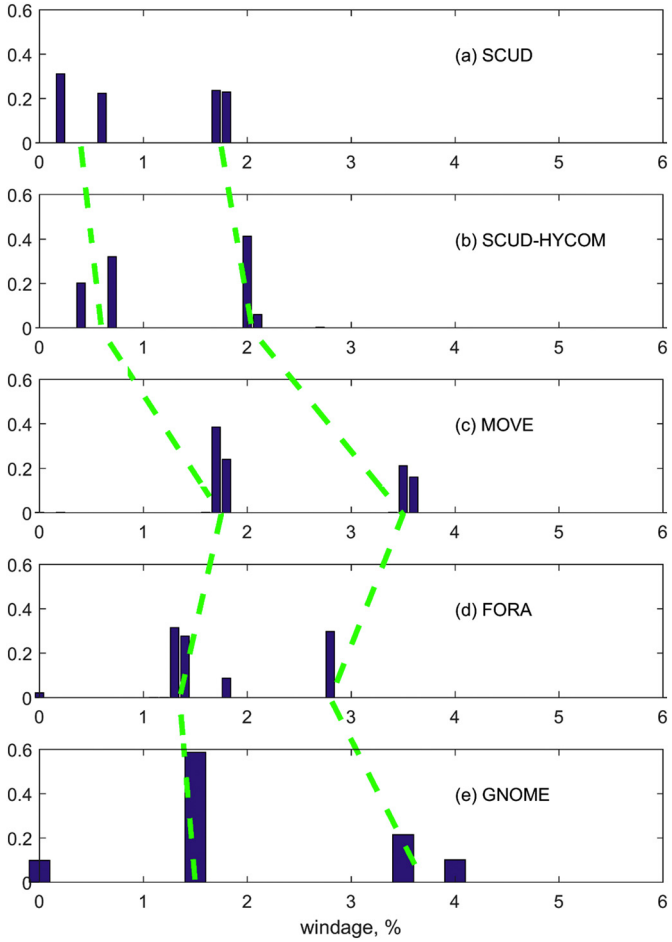

Fig. 16. Fraction of model tracer on WC in multi-windage optimization to JTMD boat reports. Green dashed lines connect groups of low- and high-windage components in different models. (For interpretation of the references to color in this figure legend, the reader is referred to the web version of this article.)

models predict that JTMD boats will continue to float in the ocean and eventually wash on shore.

A similar estimate based on the data in Table 1, gives an e-folding time for reports from the West Coast of 2.27 years and from the sea of 4.85 years. The difference between these two decay rates is consistent with the higher probability for high-windage boats to wash on shore and low-windage boats to remain in the water. These approximations predict that in year 2018, 3 to 4 JTMD boats will be reported from the West Coast and 10 to 11 from the open ocean. Collection of JTMD reports will continue to be important in verifying the numerical model solutions.

6. Summary and discussion

Numerical drift models provide a conceptual view and fill the gaps between sparse observations of marine debris. Solutions of the five different models used in this study to simulate the movement of JTMD agree qualitatively on the different pathways and fates of floating debris with different windages. All model solutions suggest that during the eastward drift from Japan, debris became stratified by wind according to its windage. High-windage items reached North America at the end of 2011 and in 2012, medium-windage recirculated southwest toward Hawaii and Asia, and low-windage debris collected in the Subtropical Gyre, primarily in the garbage patch located northeast of Hawaii.

Several methods have been developed in this study to verify model simulations quantitatively with observational reports. To reduce effects of unknown parameters, the study focused on JTMD boats. A new MD-test identified model windage values, providing the best correspondence with at-sea reports of floating boats, whose location though, may be heavily biased in favor of shipping lanes. Particular attention was paid to the model-report comparison on the North American coastline between 40 and 51°N. Model fluxes were used to identify optimal tracer windages in three scenarios: single windage, a range of windages, and an arbitrary set of windages. In the first two cases, all model runs corresponded best with observations in the 1% to 2% windage range. In the multi-windage analysis, all model solutions corresponded to observations best when run with pairs of low and medium windages, separated by approximately 1.5%.

When all tests are considered, SCUD model solutions agree better with JTMD boat reports than the solutions of the other models. It successfully reproduced primary and secondary peaks in the timeline of reports from the West Coast, shows the smallest rms deviations from reports, and demonstrated consistency between the different analyses. Despite expectations, blending SCUD in coastal areas with HYCOM did not improve SCUD's performance. The solutions of FORA, the model built on a 4dVAR technology, also agreed well with observations and, despite its coarse resolution in the eastern North Pacific, produced results close to SCUD in most quantitative evaluations. MOVE (a 3dVAR system) simulated well the drift of JTMD in 2011–2012 in the northwestern North Pacific, but its forecast after July 1, 2013, was poor and disagreed with observations.

GNOME's performance was poorer than the other models. Based on particle trajectories, the system requires much computing time so that it was run with fewer windages. Despite the very large number of particles (over 400,000) and significant “random walk,” the GNOME solution covered some areas with extremely high particle concentration, leaving other large areas completely or nearly empty. Unlike the other models, whose solutions show how smaller-scale and higher-frequency details evolve into larger scale patterns and longer timelines, GNOME solutions for boats floating in the ocean have heterogeneous and highly anisotropic structures and show very strong spills on the West Coast over relatively short time periods. GNOME solutions did not reproduce most of the observed JTMD peaks and lagged behind other models in the quantitative criteria. Comparison with SCUD-HYCOM (Fig. 2) suggests that underlying problems are not related to GNOME as a particle-launching system but result from errors in surface currents (HYCOM) or the wind stress (NOAA SeaWinds), used to force GNOME.

When simulating the dynamics of the North Pacific garbage patch, Potemra (2012) also found that the HYCOM solution was less structured than other models with noisy features on relatively small scales. In theory, the very high resolution of HYCOM solutions should reflect the mesoscale ocean dynamics. However, Douglass and Ngodock (2016) showed that the short-lived eddies and their motion in HYCOM are inconsistent with the long-lived eddies in a study by Chelton et al. (2011) or with the basic dynamics on the β plane. Because HYCOM is used by the US Navy and other agencies to coordinate critical operational activities, the results here indicate that a re-evaluation and improvement of its performance are needed.

Together the five models suggest that the Great Japan Tsunami of 2011 washed about 1000 boats off shore and that a significant fraction of these boats is still floating in the ocean and will continue washing up on North American shores in years to come. This conclusion is consistent with the preliminary estimates of Maximenko et al. (2015).

Many aspects of the modeling require improvement. Surface currents are not measured by the existing observing system and their description in ocean circulation models, which have a coarse vertical resolution (Bourassa et al., 2016) and use simple mixed-layer parameterizations, is incomplete. Wind effects on a floating object are complex and may require more adequate representation in drift models than a mere addition of a fraction of the wind vector. Changes in

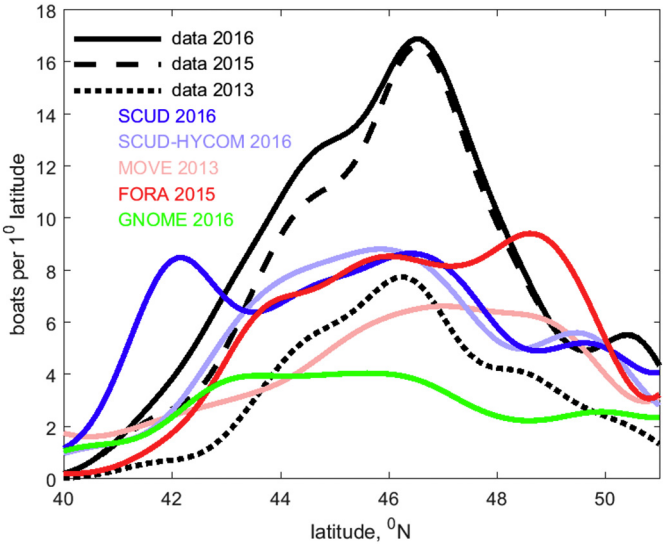

Fig. 17. Distribution with latitude of JTMD boat reports from the North America west coast and from scaled solutions of five numerical models at optimal windage parameter values, smoothed with a Gaussian filter with a 1° latitude half-width. Results are plotted for periods ending July 1, 2013 (MOVE), end of 2015 (FORA) and end of 2016 (SCUD, SCUD-HYCOM and GNOME). Observational data, corresponding to these periods are presented by black dotted, dashed and solid lines. Units are number of boats per one degree latitude.

Table 3
Estimates of total numbers of boats on West Coast and at the source for a single-windage optimization and e-folding decay scale.

	Reports	Model boats on West Coast	Fraction of tracer on West Coast	Model boats at source		E-folding time scale, years
				Best fit	Scaled with number of reports	
	i	*ii*	*iii*	*Iv*	*v*	*vi*
SCUD	92	69.5	0.136	511	676	3.85
SCUD-HYCOM	92	60.1	0.083	724	1108	2.81
MOVE	38	26.4	0.039	677	974	–
FORA	84	63.6	0.069	921	1217	8.32

windage over time due to biofouling, degradation, changes in orientation or submersion, will affect model solutions. Of particular importance is how the models are initialized. It took days to weeks for the JTMD to drift away from coastal regions and disperse, a phenomenon that requires high-resolution models for adequate simulation. Thus, very high-resolution local models would be needed to simulate the entire evolution, including re-circulation and re-floatation of JTMD stranded by storms or high tides in coastal areas.

Although anthropogenic marine debris can be found in all parts of the world's oceans, coherent datasets are largely unavailable. This is partly due to the complex composition of debris, the primitive methods practiced in data collection, and the absence of commonly accepted standards for data collection. Jambeck et al. (2015) estimate that people add 8 million tons of plastic debris to the global ocean every year, creating one of the most urgent ecological problems facing the planet. However huge these numbers are, in only one day on March 11, 2011, the Great Japan Tsunami generated east of Honshu about 1.5 million tons of floating debris (estimate by the Japan Ministry of the Environment), an amount comparable to the total annual debris budget of the entire North Pacific. One to two years later, the influx of debris on Washington State shorelines increased as much as ten times (Murray et al., 2018). However, because much of JTMD looked similar to the usual people-generated debris, only a fraction of JTMD items could be confidently traced back to the tsunami.

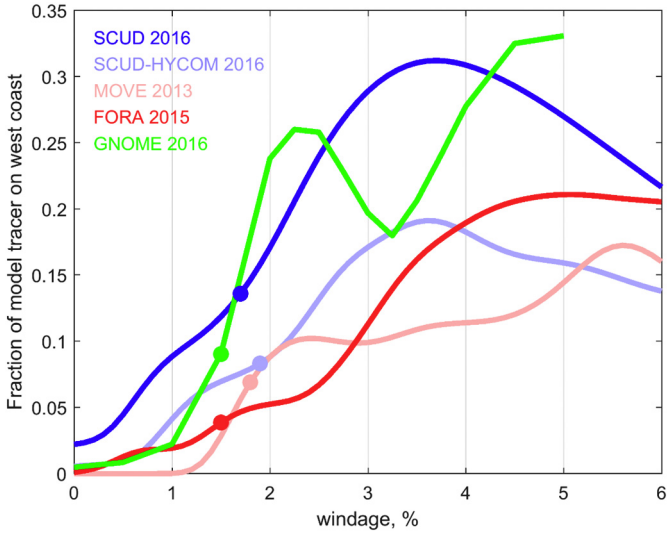

Fig. 18. Fraction of model tracer with different windages that accumulated on the North America west coastline between 40 and 51°N by July 1, 2013 (for MOVE), end of 2015 (for FORA), and end of 2016 (for SCUD, SCUD-HYCOM, and GNOME). Filled circles mark optimal windage parameter values for different models (Fig. 11).

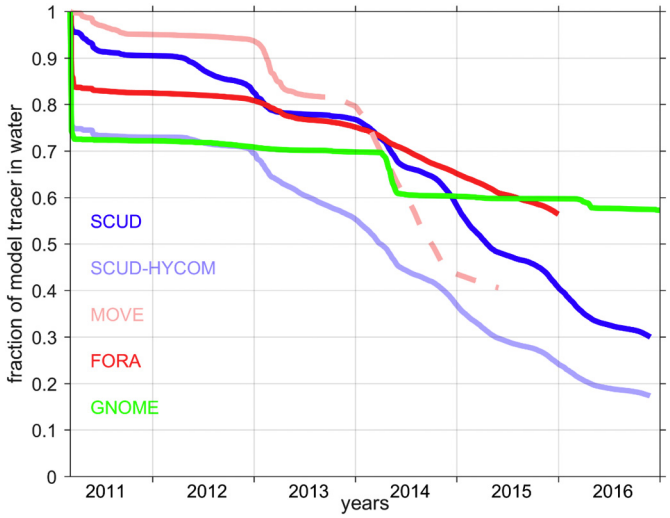

Fig. 19. Fraction of tracer remaining "in water" in single-windage optimal model solutions as a function of time.

Development of the marine debris observing system is important to improve drift models. Such a system must include observations of areas both with and without debris to reveal patterns of debris clusters. The following improvements are needed: include continuous measurements with a variety of sensors that cover different types of marine debris in different environments (i.e. water and shore); unbiased distribution of observational reports; correction for time lag between item shore-arrival and detection; and better knowledge of source-distribution and debris-composition. Currently, we do not know whether the index based on numbers of damaged homes reflects adequately the number of JTMD boats within the model boundaries.

The costs of improving the observing system and models are justified by the broad range of applications that will benefit, including but not limited to drifts of oil spills, sea ice and icebergs, advection of marine biota and transport of alien species, maritime safety and search

and rescue operations. For example, the methods and models developed in this JTMD study were successfully used by Duhec et al. (2015) to describe the source and pathways of general marine debris in the Indian Ocean that ends up on the shores of the Seychelles Islands and also by Trinanes et al. (2016) to determine the possible drift of debris from the Malaysian Airlines Flight 370. Generally, to make mankind's ocean-related activities safer, the motions of objects floating on the ocean surface and of matter dissolved or suspended in the ocean's upper layer need to be better monitored and understood.

Acknowledgements

The project ADRIFT was managed in 2014–2017 by the North Pacific Marine Science Organization (PICES) and funded by the Ministry of the Environment (MoE) of Japan (Murray et al., 2015). The Japan modeling group acknowledges support from the Japan Office of Ocean Policy and MoE in conducting the JTMD simulations. Help with the data acquisition from Lexter Tapawan, Nir Barnea, Peter Murphy (NOAA), Barbara Lee (DLNR), Gisela Speidel, Kin Lik Wang, and Christina Curto (IPRC) as well as from many private contributors is gratefully acknowledged. We also appreciate the help of Dr. Maki with obtaining the data on the number of homes destroyed by the Great Japan Tsunami. We thank two anonymous reviewers and Cathryn Clarke Murray for their comments that helped to significantly improve the manuscript. The SCUD model was built with partial support from the NASA Ocean Surface Topography Science Team (OSTST). The model data used in this study are available at http://iprc.soest.hawaii.edu/MarineDebrisModels/. This is IPRC/SOEST Publication 1319/10355.

References

Bleck, R., Boudra, D., 1981. Initial testing of a numerical ncean circulation model using a hybrid (quasi-isopycnic) vertical coordinate. J. Phys. Oceanogr. 11, 755–770.

Bourassa, M., Morey, S.L., Xie, S.-P., Chelton, D., Samuelson, R., Farrar, T., Maximenko, N., Thompson, A., 2016. Wind and Current Coupling, White Paper for the Earth Science and Applications from Space Decadal Survey, RFI1.

Carlton, J.T., Chapman, J.W., Geller, J.B., Miller, J.A., Carlton, D.A., McCuller, M.I., Treneman, N.C., Steves, B.P., Ruiz, G.M., 2017. Tsunami-driven rafting: transoceanic species dispersal and implications for marine biogeography. Science 357 (6358), 1402–1406.

Chelton, D.B., Schlax, M.G., Samelson, R.M., 2011. Global observations of nonlinear mesoscale eddies. Prog. Oceanogr. 91 (2), 167–216. http://dx.doi.org/10.1016/j.pocean.2011.01.002.

Douglass, E., Ngodock, H., 2016. Persistance and Propagation of Eddies in High-Resolution Data-Assimilating Models, Presentation at 2016 Ocean Sciences Meeting, February 21–26, 2016, New Orleans, Louisiana.

Duhec, A.V., Jeanne, R.F., Maximenko, N.A., Hafner, J., 2015. Composition and potential origin of marine debris stranded in the Western Indian Ocean on remote Alphonse Island, Seychelles. Mar. Pollut. Bull. 96 (1–2), 76–86. http://dx.doi.org/10.1016/j.marpolbul.2015.05.042.

Eriksen, M., Maximenko, N.A., Thiel, M., Cummins, A., Lattin, G., Wilson, S., Hafner, J., Zellers, A., Rifman, S., 2013. Plastic pollution in the South Pacific subtropical gyre. Mar. Pollut. Bull. 68 (1–2), 71–76. http://dx.doi.org/10.1016/j.marpolbul.2012.12.021.

Jambeck, J.R., Geyer, R., Wilcox, C., Siegler, T.R., Perryman, M., Andrady, A., Narayan, R., Law, K.L., 2015. Plastic waste inputs from land into the ocean. Science 347, 768. http://dx.doi.org/10.1126/science.1260352.

Japan Ministry of Environment, 2014. A Report on Forecasts of Tsunami Driftage Location (March, 7 pp.). http://www.kantei.go.jp/jp/singi/kaiyou/hyouryuu_eng/gaiyou.pdf.

Kako, S., Isobe, A., Kataoka, T., Yufu, K., Sugizono, S., Plybon, C., Murphy, T.A., 2018. Sequential Webcam Monitoring and Modeling of Marine Debris Abundance on a Beach on the Western US Coast. (this issue).

Kawamura, H., Kobayashi, T., Nishikawa, S., Ishikawa, Y., Usui, N., Kamachi, M., Aso, N., Tanaka, Y., Awaji, T., 2014. Drift simulation of tsunami debris in the North Pacific. Glob. Environ. Res. 18 (1), 81–96.

Kubota, M., 1994. A mechanism of the accumulation of floating marine debris north of Hawaii. J. Phys. Oceanogr. 24, 1059–1064.

Law, K.L., Morét-Ferguson, S., Maximenko, N.A., Proskurowski, G., Peacock, E.E., Hafner, J., Reddy, C.M., 2010. Plastic accumulation in the North Atlantic Subtropical Gyre. Science 329, 1185–1188.

Maximenko, N.A., Hafner, J., 2010. SCUD: Surface Currents from Diagnostic model, IPRC Tech. Note 5 (17 pp.). http://apdrc.soest.hawaii.edu/projects/SCUD/SCUD_manual_02_17.pdf.

Maximenko, N.A., Hafner, J., Niiler, P., 2012. Pathways of marine debris from trajectories of Lagrangian drifters. Mar. Pollut. Bull. 65 (1–3), 51–62. http://dx.doi.org/10.1016/j.marpolbul.2011.04.016.

Maximenko, N., MacFadyen, A., Kamachi, M., 2015. Modeling Drift of Marine Debris from the Great Tohoku Tsunami. Vol. 23, No. 2. PICES Press, Summer 2015, pp. 32–36.

Maximenko, N., Niiler, P., Rio, M.-H., Melnichenko, O., Centurioni, L., Chambers, D., Zlotnicki, V., Galperin, B., 2009. Mean dynamic topography of the ocean derived from satellite and drifting buoy data using three different techniques. J. Atmos. Ocean. Technol. 26 (9), 1910–1919.

Ministry of the Environment, Japanese Agency, 2012. Estimated Total Amount of Debris Washed Out by the Great East Japan Earthquake. http://www.env.go.jp/en/focus/docs/files/20120901-57.pdf.

Moore, C., Moore, S.L., Leecaster, M.K., Weisberg, S.B., 2001. A comparison of plastic and plankton in the north pacific central gyre. Mar. Pollut. Bull. 42 (12), 1297–1300. http://dx.doi.org/10.1016/S0025-326X(01)00114-X. (2001-12-01).

Moy, K., Neilson, B., Chung, A., Meadows, A., Castrence, M., Ambagis, S., Davidson, K., 2017. Mapping coastal marine debris using aerial imagery and spatial analysis. Mar. Poll. Bull. http://dx.doi.org/10.1016/j.marpolbul.2017.11.045. (this issue).

Murray, C.C., Bychkov, A., Therriault, T., Maki, H., Wallace, N., 2015. The Impact of Japanese Tsunami Debris on North America. Vol. 23, No. 1. PICES Press, pp. 28–30.

Murray, C.C., Maximenko, N., Lippiatt, S., 2018. The influx of marine debris from the Great Japan Tsunami of 2011 to North American shorelines. Mar. Pollut. Bull. http://dx.doi.org/10.1016/j.marpolbul.2018.01.004. (this issue).

Niiler, P.P., Maximenko, N.A., Panteleev, G.G., Yamagata, T., Olson, D.B., 2003. Near-surface dynamical structure of the Kuroshio Extension. J. Geophys. Res. 108 (C6), 3193. http://dx.doi.org/10.1029/2002JC001461.

Potemra, J.T., 2012. Numerical modeling with application to tracking marine debris. Mar. Pollut. Bull. 65 (1–3), 42–50. http://dx.doi.org/10.1016/j.marpolbul.2011.06.026.

van Sebille, E., Wilcox, C., Lebreton, L., Maximenko, N.A., Hardesty, B.D., van Franeker, J.A., Eriksen, M., Siegel, D., Galgani, F., Law, K.L., 2015. A global inventory of small floating plastic debris. Environ. Res. Lett. 10 (12), 124006. http://dx.doi.org/10.1088/1748-9326/10/12/124006.

Sugiura, N., Awaji, T., Masuda, S., Mochizuki, T., Toyoda, T., Miyama, T., Igarashi, H., Ishikawa, Y., 2008. Development of a 4-dimensional variational coupled data assimilation system for enhanced analysis and prediction of seasonal to interannual climate variations. J. Geophys. Res. 113, C10017. http://dx.doi.org/10.1029/2008JC004741.

Trinanes, J.A., Olascoaga, M.J., Goni, G.J., Maximenko, N.A., Griffin, D.A., Hafner, J., 2016. Analysis of potential MH370 debris trajectories using ocean observations and numerical model results. J. Operation. Oceanography 9 (2), 126–138. http://dx.doi.org/10.1080/1755876X.2016.1248149.

Tsujino, H., Motoi, T., Ishikawa, I., Hirabara, M., Nakano, H., Yamanaka, G., Yasuda, T., Ishizaki, H., 2010. Reference manual for the meteorological research institute community ocean model (mri.com) version 3. In: Tech. Rep. 59, Meteorol. Res. Inst., Tsukuba, Japan.

Usui, N., Fujii, Y., Sakamoto, K., Kamachi, M., 2015. Development of a four-dimensional variational assimilation system for coastal data assimilation around Japan. Mon. Weather Rev. 143, 3874–3892.

Usui, N., Ishizaki, S., Fujii, Y., Tsujino, H., Yasuda, T., Kamachi, M., 2006. Meteorological Research Institute multivariate ocean variational estimation (MOVE) system: some early results. Adv. Spa. Res. 37, 806–822.

Usui, N., Wakamatsu, T., Tanaka, Y., Hirose, N., Toyoda, T., Nishikawa, S., Fujii, Y., Takatsuki, Y., Igarashi, H., Nishikawa, H., Ishikawa, Y., Kuragano, T., Kamachi, M., 2017. Four-dimensional variational ocean reanalysis: a 30-year high-resolution dataset in the western North Pacific (FORA-WNP30). J. Oceanogr. 73, 205–233. http://dx.doi.org/10.1007/s10872-016-0398-5.